

Diffusion of impurities in a moderately dense confined granular gas

Rubén Gómez González,^{1, a)} Vicente Garzó,^{2, b)} Ricardo Brito,^{3, c)} and Rodrigo Soto^{4, d)}

¹⁾Departamento de Didáctica de las Ciencias Experimentales y las Matemáticas, Universidad de Extremadura, E-10004 Cáceres, Spain

²⁾Departamento de Física and Instituto de Computación Científica Avanzada (ICCAEx), Universidad de Extremadura, E-06071 Badajoz, Spain

³⁾Departamento de Estructura de la Materia, Física Térmica y Electrónica and GISC, Universidad Complutense de Madrid, E-28040 Madrid, Spain

⁴⁾Departamento de Física, Facultad de Ciencias Físicas y Matemáticas, Universidad de Chile, 8370449 Santiago, Chile

(Dated: 25 October 2024)

Mass transport of impurities immersed in a confined quasi-two-dimensional moderately dense granular gas of inelastic hard spheres is studied. The effect of the confinement on granular particles is modeled through a collisional model (the so-called Δ -model) that includes an effective mechanism to transfer the kinetic energy injected by vibration in the vertical direction to the horizontal degrees of freedom of grains. The impurity can differ in mass, diameter, inelasticity, or the energy injection at collisions, compared to the gas particles. The Enskog–Lorentz kinetic equation for the impurities is solved via the Chapman–Enskog method to first order in spatial gradients for states close to the homogeneous steady state. As usual, the three diffusion transport coefficients for tracer particles in a mixture are given in terms of the solutions of a set of coupled linear integral equations which are solved by considering the lowest Sonine approximation. The theoretical predictions for the tracer diffusion coefficient (relating the mass flux with the gradient of the number density of tracer particles) are compared with both direct simulation Monte Carlo and molecular dynamics simulations. The agreement is in general good, except for strong inelasticity and/or large contrast of energy injection at tracer-gas collisions compared to gas-gas collisions. Finally, as an application of our results, the segregation problem induced by both a thermal gradient and gravity is exhaustively analyzed.

I. INTRODUCTION

The study of transport properties of granular gases (modeled as a gas of hard spheres undergoing inelastic collisions) confined in a given direction is still a challenging open problem. In particular, one geometry that has attracted the attention of many researchers is the so-called quasi-two-dimensional geometry, namely, when the granular gas is confined in a box whose vertical z -direction is slightly larger than one particle diameter.^{1–3} When the box is subjected to vertical vibrations, energy is injected into the vertical degrees of freedom of the particles as they collide with the plates of the system. This kinetic energy gained by the particles is then transferred to the particles' horizontal degrees of freedom when they collide with each other. Under certain conditions, it has been observed that the system maintains a homogeneous fluidized state (as viewed from above) over a wide range of parameters.⁴

However, a kinetic theory description of the above confined system is quite intricate due basically to the restrictions imposed by the confinement in the corresponding Boltzmann collisional operator. Thus, although several attempts have been recently made by considering

the above approach,^{5–7} one can consider in a more effective way the effect of the confinement on the dynamics of granular particles via the collisional model proposed in Ref.8. The idea behind this collisional model is that the magnitude of the normal component of the relative velocity of the colliding particles is increased by a constant factor Δ in each collision. The term associated with the factor Δ in the corresponding collisional rule tries to mimic the transfer of kinetic energy from the vertical degrees of freedom of granular particles to the horizontal ones. This sort of collisional model will be referred to here as the Δ -model.

The Δ -model has been employed extensively in recent years to study monocomponent granular gases. It has been applied to analyze the homogeneous state,^{9,10} to obtain the Navier–Stokes transport coefficients,¹¹ and to perform stability analyses of the time-dependent homogeneous state.¹² Independently, the shear viscosity coefficient of a dilute granular gas has been explicitly calculated and shows good agreement with computer simulations.¹³ Extensions of these works to moderate densities, within the framework of the Enskog kinetic equation, have also been reported in several papers.^{14–16} In addition, the Δ -model has been employed in the study of systems with long-range interactions,¹⁷ absorbing states,¹⁸ and the formation of quasi-long-range ordered phases.^{19,20}

More recently, the Δ -model has been also used to determine the Navier–Stokes transport coefficients of *dilute* binary granular mixtures.²¹ As an application of this result, the stability analysis of the so-called homogeneous

^{a)}Electronic mail: ruben@unex.es

^{b)}Electronic mail: vicenteg@unex.es; <https://fisteor.cms.unex.es/investigadores/vicente-garzo-puertos/>

^{c)}Electronic mail: brito@ucm.es

^{d)}Electronic mail: rsoto@uchile.cl

steady state (HSS) and the segregation problem driven by both a thermal gradient and gravity have been also studied in a subsequent paper.^{22,23} For now, the study of binary mixtures has only considered the Boltzmann kinetic equation as the starting point and so, they are restricted to the low-density regime. Thus, it is quite natural to extend the analysis performed in Ref. 21 to the (revised) Enskog kinetic theory for a description of hydrodynamics and transport at higher densities.

Needless to say, the evaluation of the Navier–Stokes transport coefficients for a *dense* granular mixture is quite an intricate problem, due mainly to the coupling between the different integral equations obeying the complete set of transport coefficients. Thus, to gain some insight into the general problem, we will make here a first approach to the description of a general mixture by considering a more simple situation: we consider a granular binary mixture where the concentration of one of the species (of mass m_0 and diameter σ_0) is very small (impurity or tracer limit). In this situation, one can assume that (i) the state of the dense granular gas (excess species of mass m and diameter σ) is not perturbed by the presence of tracer particles, and (ii) one can also neglect collisions among tracer particles themselves in their corresponding kinetic equation. Under these conditions, the velocity distribution function f of the granular gas obeys a (closed) nonlinear Enskog equation while the velocity distribution function f_0 of the tracer particles verifies a linear Enskog–Lorentz equation. At a kinetic level, the tracer limit greatly simplifies the application of the Chapman–Enskog method²⁴ to a multicomponent granular mixture.

Since in the tracer limit the pressure tensor and the heat flux of the mixture (impurities or tracer particles plus granular gas) are the same as that for the excess species,¹⁴ the mass transport of impurities \mathbf{j}_0 is the relevant flux of the problem. For symmetry reasons, the Navier–Stokes constitutive equation for the mass flux (that is, linear in the spatial gradients) is given by

$$\mathbf{j}_0^{(1)} = -\frac{m_0^2}{\rho} D_0 \nabla n_0 - \frac{mm_0}{\rho} D \nabla n - \frac{\rho}{T} D_T \nabla T, \quad (1)$$

where $\rho = mn$ is the total mass density of the granular gas, n_0 is the number density of the tracer particles, n is the number density of the gas particles, and T is the granular temperature. In addition, D_0 is the tracer diffusion coefficient, D is the mutual diffusion coefficient, and D_T is the thermal diffusion coefficient. The determination of the diffusion transport coefficients D_0 , D , and D_T is the main objective of the present work. As for elastic collisions,²⁴ these transport coefficients are given in terms of the solutions of a set of coupled linear integral equations. These integral equations are approximately solved by considering the leading terms in a Sonine polynomial expansion. However, as in the case of dilute granular mixtures,²¹ evaluating the diffusion coefficients in the time-dependent problem requires numerically solving a set of nonlinear differential equations. To simplify the

analysis, we focus here on the relevant state of confined systems with *steady* granular temperature. This steady state allows for a more tractable approach and enables the derivation of analytical expressions for D_0 , D , and D_T in terms of the parameter space of the system.

To assess the accuracy of the (approximate) theoretical results, kinetic theory predictions for the tracer diffusion coefficient D_0 obtained in the first Sonine approximation are confronted against computer simulations carried out independently by both molecular dynamics (MD)^{25–27} and the direct simulation Monte Carlo (DSMC) method.²⁸ As in previous works,^{29,30} the diffusion coefficient is computed in the simulations from the mean-square displacement (MSD) of impurities immersed in a confined dense granular gas undergoing the homogeneous steady state (HSS).

Finally, since the explicit forms of the diffusion transport coefficients are at hand, a segregation criterion based on the thermal diffusion factor is derived. Segregation, induced by both gravity and a thermal gradient, shows the transition between the so-called Brazil-nut effect (BNE) and the reverse Brazil-nut effect (RBNE) by varying the parameters of the system. As expected, the corresponding phase diagrams characterizing the transition BNE/RBNE are different from those previously obtained for inelastic hard spheres or disks (IHS).^{30,31}

The plan of the paper is as follows. The Δ -model and the Enskog equation are introduced in Sec. II for the granular gas while Sec. III deals with the Enskog–Lorentz kinetic equation for the tracer particles. The application of the Chapman–Enskog method to solve the Enskog–Lorentz equation to first order in spatial gradients is described in Sec. IV. The corresponding integral equations obeying the diffusion transport coefficients are also derived. Then, these integral equations are approximately solved up to the first Sonine approximation in Sec. V. Some technical details of the calculations are provided in the Appendices A and B. The theoretical results for the tracer diffusion coefficient D_0 are compared with both DSMC results and MD simulations for several configurations in Sec. VI. Thermal diffusion segregation is analyzed in Sec. VII, while the paper is closed in Sec. VIII with a brief discussion of the reported results.

II. ENSKOG KINETIC EQUATION FOR A MODEL OF A CONFINED QUASI-TWO DIMENSIONAL GRANULAR GAS AT MODERATE DENSITIES

A. Collision rules in the Δ -model

We consider a set of solid particles or grains of mass m and diameter σ . Under rapid flow conditions, the set can be modeled as a gas of hard spheres with inelastic collisions. In the simplest case, the spheres are assumed to be completely smooth and hence, the inelasticity in collisions is characterized by the (positive) constant coefficient of normal restitution α . As said in the Introduction,

here we start from a collisional model (the Δ -model) for a quasi-two dimensional geometry where grains are confined in the vertical direction. In this model, an extra velocity Δ (which is assumed to be constant) is added to the relative motion of the colliding spheres in such a way the magnitude of the normal component of the relative velocity is increased by a given factor in each binary collision. Thus, the relationship between the pre-collisional velocities ($\mathbf{v}_1, \mathbf{v}_2$) and the post-collisional velocities ($\mathbf{v}'_1, \mathbf{v}'_2$) in the Δ -model is⁸

$$\mathbf{v}'_1 = \mathbf{v}_1 - \frac{1}{2} (1 + \alpha) (\hat{\boldsymbol{\sigma}} \cdot \mathbf{g}_{12}) \hat{\boldsymbol{\sigma}} - \Delta \hat{\boldsymbol{\sigma}}, \quad (2)$$

$$\mathbf{v}'_2 = \mathbf{v}_2 + \frac{1}{2} (1 + \alpha) (\hat{\boldsymbol{\sigma}} \cdot \mathbf{g}_{12}) \hat{\boldsymbol{\sigma}} + \Delta \hat{\boldsymbol{\sigma}}, \quad (3)$$

where $\mathbf{g}_{12} = \mathbf{v}_1 - \mathbf{v}_2$ is the relative velocity and $\hat{\boldsymbol{\sigma}}$ is the unit collision vector joining the centers of the two colliding spheres and pointing from particle 1 to particle 2. Particles are approaching if $\hat{\boldsymbol{\sigma}} \cdot \mathbf{g}_{12} > 0$. In Eqs. (2) and (3), α is the (constant) coefficient of normal restitution defined in the interval $0 < \alpha \leq 1$, and Δ (which has dimensions of velocity) is positive. This extra velocity is compatible with angular momentum conservation³² and points outward in the normal direction $\hat{\boldsymbol{\sigma}}$. From Eqs. (2) and (3) is quite simple to get the relative velocity after collision \mathbf{g}'_{12} as

$$\mathbf{g}'_{12} = \mathbf{v}'_1 - \mathbf{v}'_2 = \mathbf{g}_{12} - (1 + \alpha) (\hat{\boldsymbol{\sigma}} \cdot \mathbf{g}_{12}) \hat{\boldsymbol{\sigma}} - 2\Delta \hat{\boldsymbol{\sigma}}, \quad (4)$$

so that

$$(\hat{\boldsymbol{\sigma}} \cdot \mathbf{g}'_{12}) = -\alpha (\hat{\boldsymbol{\sigma}} \cdot \mathbf{g}_{12}) - 2\Delta. \quad (5)$$

The collision rules (2) and (3) conserve momentum but energy is not conserved. The change in kinetic energy

upon collision is

$$\begin{aligned} \Delta E &\equiv \frac{m}{2} (v'_1'^2 + v'_2'^2 - v_1^2 - v_2^2) \\ &= m \left[\Delta^2 + \alpha \Delta (\hat{\boldsymbol{\sigma}} \cdot \mathbf{g}_{12}) - \frac{1 - \alpha^2}{4} (\hat{\boldsymbol{\sigma}} \cdot \mathbf{g})^2 \right]. \end{aligned} \quad (6)$$

The right-hand side of Eq. (6) vanishes for elastic collisions ($\alpha = 1$) and $\Delta = 0$. According to Eq. (6), $\Delta E > 0$ (energy is gained in a binary collision) if $\hat{\boldsymbol{\sigma}} \cdot \mathbf{g}_{12} < 2\Delta/(1 - \alpha)$ while $\Delta E < 0$ (energy is lost in a binary collision) if $\hat{\boldsymbol{\sigma}} \cdot \mathbf{g}_{12} > 2\Delta/(1 - \alpha)$.

For practical purposes, it is also convenient to consider the restituting collision $(\mathbf{v}''_1, \mathbf{v}''_2) \rightarrow (\mathbf{v}_1, \mathbf{v}_2)$ with the same collision vector $\hat{\boldsymbol{\sigma}}$:

$$\mathbf{v}''_1 = \mathbf{v}_1 - \frac{1}{2} (1 + \alpha^{-1}) (\hat{\boldsymbol{\sigma}} \cdot \mathbf{g}_{12}) \hat{\boldsymbol{\sigma}} - \alpha^{-1} \Delta \hat{\boldsymbol{\sigma}}, \quad (7)$$

$$\mathbf{v}''_2 = \mathbf{v}_2 + \frac{1}{2} (1 + \alpha^{-1}) (\hat{\boldsymbol{\sigma}} \cdot \mathbf{g}_{12}) \hat{\boldsymbol{\sigma}} + \alpha^{-1} \Delta \hat{\boldsymbol{\sigma}}. \quad (8)$$

The volume transformation in velocity space in a direct collision is $d\mathbf{v}'_1 d\mathbf{v}'_2 = \alpha d\mathbf{v}_1 d\mathbf{v}_2$, and so $d\mathbf{v}''_1 d\mathbf{v}''_2 = \alpha^{-1} d\mathbf{v}_1 d\mathbf{v}_2$.

B. Enskog kinetic equation

We assume that the granular gas is in the presence of a gravitational field \mathbf{g} . At a kinetic level, all the relevant information on the state of the system is provided by the knowledge of the one-particle velocity distribution function $f(\mathbf{r}, \mathbf{v}; t)$. For moderate densities, this distribution verifies the Enskog kinetic equation^{8,9}

$$\frac{\partial f}{\partial t} + \mathbf{v} \cdot \nabla f + \mathbf{g} \cdot \frac{\partial f}{\partial \mathbf{v}} = J[\mathbf{r}, \mathbf{v}; f, f], \quad (9)$$

where the Enskog collision operator J of the Δ -model reads

$$\begin{aligned} J[\mathbf{r}, \mathbf{v}_1; f, f] &\equiv \sigma^{d-1} \int d\mathbf{v}_2 \int d\hat{\boldsymbol{\sigma}} \Theta(-\hat{\boldsymbol{\sigma}} \cdot \mathbf{g}_{12} - 2\Delta) (-\hat{\boldsymbol{\sigma}} \cdot \mathbf{g}_{12} - 2\Delta) \alpha^{-2} \chi(\mathbf{r}, \mathbf{r} + \boldsymbol{\sigma}) f(\mathbf{r}, \mathbf{v}_1''; t) \\ &\quad \times f(\mathbf{r} + \boldsymbol{\sigma}, \mathbf{v}_2''; t) - \sigma^{d-1} \int d\mathbf{v}_2 \int d\hat{\boldsymbol{\sigma}} \Theta(\hat{\boldsymbol{\sigma}} \cdot \mathbf{g}_{12}) (\hat{\boldsymbol{\sigma}} \cdot \mathbf{g}_{12}) \chi(\mathbf{r}, \mathbf{r} + \boldsymbol{\sigma}) f(\mathbf{r}, \mathbf{v}_1; t) f(\mathbf{r} + \boldsymbol{\sigma}, \mathbf{v}_2; t). \end{aligned} \quad (10)$$

Like the Boltzmann equation, the Enskog equation neglects velocity correlations among particles that are about to collide, but it accounts for excluded volume effects through the pair correlation function $\chi(\mathbf{r}, \mathbf{r} \pm \boldsymbol{\sigma})$. In Eq. (10), $\Theta(x)$ is the Heaviside step function and d is the

dimensionality of the system ($d = 2$ for disks and $d = 3$ for spheres). Note that although the system considered is two-dimensional, the calculations worked out here will be performed by an arbitrary number of dimensions d .

An important property of the Enskog collision operator is^{9,13}

$$\begin{aligned}
I_\psi &\equiv \int d\mathbf{v}_1 \psi(\mathbf{v}_1) J[\mathbf{r}, \mathbf{v}_1 | f, f] \\
&= \sigma^{d-1} \int d\mathbf{v}_1 \int d\mathbf{v}_2 \int d\hat{\boldsymbol{\sigma}} \Theta(\hat{\boldsymbol{\sigma}} \cdot \mathbf{g}_{12}) (\hat{\boldsymbol{\sigma}} \cdot \mathbf{g}_{12}) \chi(\mathbf{r}, \mathbf{r} + \boldsymbol{\sigma}) f(\mathbf{r}, \mathbf{v}_1; t) f(\mathbf{r} + \boldsymbol{\sigma}, \mathbf{v}_2; t) [\psi(\mathbf{v}'_1) - \psi(\mathbf{v}_1)],
\end{aligned} \tag{11}$$

where \mathbf{v}'_1 is defined by Eq. (2). The property (11) is the same as for the conventional model of IHS. A consequence of the relation (11) is that the balance equations of the densities of mass, momentum, and energy can be derived by following similar mathematical steps as those made for IHS. They are given by¹⁴

$$D_t n + n \nabla \cdot \mathbf{U} = 0, \tag{12}$$

$$\rho D_t U_i + \partial_j P_{ij} = \rho \mathbf{g}, \tag{13}$$

$$D_t T + \frac{2}{dn} (\partial_i q_i + P_{ij} \partial_j U_i) = -\zeta T, \tag{14}$$

where $D_t \equiv \partial_t + \mathbf{U} \cdot \nabla$ is the material derivative, $\partial_i \equiv \partial/\partial r_i$, and $\rho = mn$ is the mass density. In terms of the distribution f , the hydrodynamic fields n , \mathbf{U} , and T are defined as

$$\{n, n\mathbf{U}, dnT\} = \int d\mathbf{v} \{1, \mathbf{v}, mV^2\} f(\mathbf{r}, \mathbf{v}; t), \tag{15}$$

where $\mathbf{V} = \mathbf{v} - \mathbf{U}$ is the peculiar velocity. The forms of the pressure tensor P_{ij} , the heat flux \mathbf{q} , and the cooling rate ζ in terms of the distribution f can be found in Ref. 14. In addition, the Enskog equation (9) has been also solved by means of the Chapman–Enskog method²⁴ and explicit expressions for the Navier–Stokes transport coefficients and the cooling rate have been derived by assuming steady state conditions.^{14,15}

C. Homogeneous steady state

We consider the HSS in the absence of the gravitational field ($\mathbf{g} = \mathbf{0}$). In this simple situation, the heat flux vanishes ($\mathbf{q} = \mathbf{0}$) and the pressure tensor $P_{ij} = p\delta_{ij}$, where the hydrostatic pressure p is given by¹⁴

$$p = nTp^*, \quad p^* = 1 + 2^{d-2} \chi \phi (1 + \alpha) + \frac{2^d}{\sqrt{2\pi}} \chi \phi \Delta^*. \tag{16}$$

In Eq. (16), the solid volume fraction ϕ is defined as

$$\phi = \frac{\pi^{d/2}}{2^{d-1} d \Gamma(\frac{d}{2})} n \sigma^d, \tag{17}$$

while $\Delta^* = \Delta/v_0$, with $v_0 = \sqrt{2T/m}$ being the thermal velocity. Note that here T means the steady state value of the granular temperature. Moreover, since $\partial_t T = 0$, Eq. (16) implies that the cooling rate $\zeta = 0$ in the HSS.

As shown in Ref. 33, a good estimate of the steady temperature is provided when ζ is evaluated by means of the Maxwellian distribution

$$f(\mathbf{v}) \rightarrow f_M(\mathbf{v}) = n \left(\frac{m}{2\pi T} \right)^{d/2} \exp \left(-\frac{mv^2}{2T} \right). \tag{18}$$

Using the approximation (18), ζ can be written as

$$\zeta = \frac{\sqrt{2\pi}^{\frac{d-1}{2}}}{d \Gamma(\frac{d}{2})} n \sigma^{d-1} v_0 \chi(\phi) \left(1 - \alpha^2 - 2\Delta^{*2} - \sqrt{2\pi} \alpha \Delta^* \right). \tag{19}$$

The condition $\zeta = 0$ yields a quadratic equation in Δ^* , whose physical solution is

$$\Delta^*(\alpha) = \frac{1}{2} \sqrt{\frac{\pi}{2}} \alpha \left[\sqrt{1 + \frac{4(1 - \alpha^2)}{\pi \alpha^2}} - 1 \right]. \tag{20}$$

As expected, from Eq. (20) one concludes that the steady state for elastic particles is only achieved for a vanishing extra velocity, that is, $\Delta^*(1) = 0$.

III. TRACER PARTICLES IMMERSED IN A CONFINED GRANULAR GAS

We suppose now that a few tracer or impurity particles of mass m_0 and diameter σ_0 are added to the granular gas. Since the concentration of the tracer species is negligibly small, their presence does not perturb the state of the granular gas. This means that the velocity distribution function $f(\mathbf{r}, \mathbf{v}; t)$ still verifies the Enskog equation (9) and so, the balance equations for the number density n , the mean flow velocity \mathbf{U} , and the temperature T for the granular gas are given by Eqs. (12), (13), and (14), respectively. In addition, as mentioned in Sec. I, in this paper we are mainly interested in the evaluation of the transport coefficients defining the mass flux of the impurities since in the tracer limit the pressure tensor and the heat flux are the same as those of the granular gas (excess component).

Under the above conditions, the velocity distribution function $f_0(\mathbf{r}, \mathbf{v}; t)$ of the tracer particles satisfies the Enskog–Lorentz kinetic equation

$$\frac{\partial f_0}{\partial t} + \mathbf{v} \cdot \nabla f_0 + \mathbf{g} \cdot \frac{\partial f_0}{\partial \mathbf{v}} = J_0[\mathbf{r}, \mathbf{v} | f, f_0], \tag{21}$$

where the Enskog–Lorentz collision operator J_0 of the Δ -model reads²¹

$$\begin{aligned}
J_0[\mathbf{r}, \mathbf{v}_1 | f, f] &\equiv \bar{\sigma}^{d-1} \int d\mathbf{v}_2 \int d\hat{\boldsymbol{\sigma}} \Theta(-\hat{\boldsymbol{\sigma}} \cdot \mathbf{g}_{12} - 2\Delta_0) (-\hat{\boldsymbol{\sigma}} \cdot \mathbf{g}_{12} - 2\Delta_0) \alpha_0^{-2} \chi_0(\mathbf{r}, \mathbf{r} + \hat{\boldsymbol{\sigma}}) f_0(\mathbf{r}, \mathbf{v}_1''; t) \\
&\quad \times f(\mathbf{r} + \hat{\boldsymbol{\sigma}}, \mathbf{v}_2''; t) - \bar{\sigma}^{d-1} \int d\mathbf{v}_2 \int d\hat{\boldsymbol{\sigma}} \Theta(\hat{\boldsymbol{\sigma}} \cdot \mathbf{g}_{12}) (\hat{\boldsymbol{\sigma}} \cdot \mathbf{g}_{12}) \chi_0(\mathbf{r}, \mathbf{r} + \hat{\boldsymbol{\sigma}}) f_0(\mathbf{r}, \mathbf{v}_1; t) f(\mathbf{r} + \boldsymbol{\sigma}, \mathbf{v}_2; t).
\end{aligned} \tag{22}$$

Here, $\bar{\boldsymbol{\sigma}} = \bar{\sigma}\hat{\boldsymbol{\sigma}}$, $\bar{\sigma} = (\sigma_0 + \sigma)/2$, $\alpha_0 \leq 1$ is the (positive) coefficient of restitution for tracer-gas collisions, and χ_0 is the pair correlation function for tracer-gas pairs at contact. Note also that in Eq. (21) the mutual interactions among the tracer particles have been neglected as compared with their interactions with the particles of the granular gas. In Eq. (22), the relationship between $(\mathbf{v}_1'', \mathbf{v}_2'')$ and $(\mathbf{v}_1, \mathbf{v}_2)$ is

$$\mathbf{v}_1'' = \mathbf{v}_1 - M(1 + \alpha_0^{-1})(\hat{\boldsymbol{\sigma}} \cdot \mathbf{g}_{12})\hat{\boldsymbol{\sigma}} - 2M\Delta_0\alpha_0^{-1}\hat{\boldsymbol{\sigma}}, \tag{23}$$

$$\mathbf{v}_2'' = \mathbf{v}_2 + M_0(1 + \alpha_0^{-1})(\hat{\boldsymbol{\sigma}} \cdot \mathbf{g}_{12})\hat{\boldsymbol{\sigma}} + 2M_0\Delta_0\alpha_0^{-1}\hat{\boldsymbol{\sigma}}, \tag{24}$$

where

$$M = \frac{m}{m + m_0}, \quad M_0 = \frac{m_0}{m + m_0}. \tag{25}$$

Equations (23)–(24) yield the relationship

$$(\hat{\boldsymbol{\sigma}} \cdot \mathbf{g}_{12}'') = -\alpha_0^{-1}(\hat{\boldsymbol{\sigma}} \cdot \mathbf{g}_{12}) - 2\Delta_0\alpha_0^{-1}, \tag{26}$$

where $\mathbf{g}_{12}'' = \mathbf{v}_1'' - \mathbf{v}_2''$.

Similarly, the collision rules for the direct collisions $(\mathbf{v}_1, \mathbf{v}_2) \rightarrow (\mathbf{v}_1', \mathbf{v}_2')$ with the same collision vector $\hat{\boldsymbol{\sigma}}$ are defined as

$$\mathbf{v}_1' = \mathbf{v}_1 - M(1 + \alpha_0)(\hat{\boldsymbol{\sigma}} \cdot \mathbf{g}_{12})\hat{\boldsymbol{\sigma}} - 2M\Delta_0\hat{\boldsymbol{\sigma}}, \tag{27}$$

$$\mathbf{v}_2' = \mathbf{v}_2 + M_0(1 + \alpha_0)(\hat{\boldsymbol{\sigma}} \cdot \mathbf{g}_{12})\hat{\boldsymbol{\sigma}} + 2M_0\Delta_0\hat{\boldsymbol{\sigma}}. \tag{28}$$

Equations (27)–(28) lead to the relationship

$$(\hat{\boldsymbol{\sigma}} \cdot \mathbf{g}_{12}') = -\alpha_0(\hat{\boldsymbol{\sigma}} \cdot \mathbf{g}_{12}) - 2\Delta_0, \tag{29}$$

where $\mathbf{g}_{12}' = \mathbf{v}_1' - \mathbf{v}_2'$.

The number density for the tracer particles is defined as

$$n_0(\mathbf{r}, t) = \int d\mathbf{v} f_0(\mathbf{r}, \mathbf{v}, t). \tag{30}$$

The impurities may freely loose or gain momentum and energy in its interactions with the particles of the granular gas. Consequently, the momentum and energy are not

invariants of the collision operator $J_0[\mathbf{v}|f_0, f]$. Only the number density n_0 is conserved; its continuity equation can be directly obtained from Eq. (21) as

$$D_t n_0 + n_0 \nabla \cdot \mathbf{U} + \frac{\nabla \cdot \mathbf{j}_0}{m_0} = 0, \tag{31}$$

where

$$\mathbf{j}_0 = m_0 \int d\mathbf{v} \mathbf{V} f_0(\mathbf{r}, \mathbf{v}, t) \tag{32}$$

is the mass flux for the impurities, relative to the local flow \mathbf{U} . Although the granular temperature T is the relevant one at a hydrodynamic level, an interesting quantity at a kinetic level is the local temperature of the intruder T_0 . This quantity measures the mean kinetic energy of the intruder. It is defined as

$$T_0(\mathbf{r}, t) = \frac{m_0}{dn_0(\mathbf{r}, t)} \int d\mathbf{v} V^2 f_0(\mathbf{r}, \mathbf{v}, t). \tag{33}$$

As confirmed by kinetic theory calculations and computer simulations,³³ the global temperature T and the intruder temperature T_0 are in general different. This means that the granular energy per particle is not equally distributed between both species of the mixture.

A. Homogeneous steady state for the impurities

Before considering inhomogeneous states for the impurities, it is convenient to characterize the HSS. This state has been widely analyzed in Ref. 33 by theoretical approaches and computer simulations. Since in the steady state $\partial_t T_0 = 0$, then [analogously to Eq. (14)] the temperature ratio T_0/T is determined from the condition $\zeta_0 = 0$. Here, ζ_0 is the cooling rate for the impurities in the HSS. As in the case of the global cooling rate ζ , a good estimate of ζ_0 can be achieved by replacing f by f_M and f_0 by the Maxwellian distribution

$$f_{0,M}(\mathbf{v}) = n_0 \left(\frac{m_0}{2\pi T_0} \right)^{d/2} \exp \left(-\frac{m_0 v^2}{2T_0} \right). \tag{34}$$

In this approximation, $\zeta_0 = \nu \zeta_0^*$ where $\nu = n\sigma^{d-1}v_0$ and ζ_0^* is³³

$$\begin{aligned}\zeta_0^* = & \frac{4\pi^{(d-1)/2}}{d\Gamma\left(\frac{d}{2}\right)} \left(\frac{\bar{\sigma}}{\sigma}\right)^{d-1} M\chi_0(1+\alpha_0)\theta^{-1/2} (1+\theta)^{1/2} \left[1 - \frac{1}{2}M(1+\alpha_0)(1+\theta)\right] \\ & - \frac{4\pi^{d/2}}{d\Gamma\left(\frac{d}{2}\right)} \left(\frac{\bar{\sigma}}{\sigma}\right)^{d-1} M\chi_0\Delta_0^* \left[\frac{2M\Delta_0^*}{\sqrt{\pi}}\theta^{1/2} (1+\theta)^{1/2} - 1 + M(1+\alpha_0)(1+\theta)\right].\end{aligned}\quad (35)$$

Here, $\Delta_0^* = \Delta_0/v_0$ and $\theta = m_0T/mT_0$ is the ratio between the mean square velocities of the impurity and particles of the granular gas.

IV. DIFFUSION TRANSPORT COEFFICIENTS

We want to determine the mass flux \mathbf{j}_0 to first-order in spatial gradients by solving the Enskog–Lorentz equation (21) by means of the Chapman–Enskog method²⁴ adapted to inelastic collisions. Thus, after a short stage where the system has forgotten its initial conditions, a hydrodynamic regime is reached where the microscopic state of the granular gas is governed by the hydrodynamic fields n_0 , n , \mathbf{U} , and T . Note that although the granular temperature is not a conserved field (due to the inelastic character of collisions), we assume that T can be still considered as a slow field. This assumption has been clearly supported by different computer simulation works.³⁴ In the hydrodynamic regime, the Enskog–Lorentz equation (21) admits a *normal* (or hydrodynamic) solution where all the space and time dependence of f_0 only occurs through a functional dependence on the hydrodynamic fields. As usual,²⁴ this functional dependence can be made explicit by assuming small spatial gradients. In this case, f_0 can be written as a series expansion in powers of the spatial gradients of the hydrodynamic fields:

$$f_0 = f_0^{(0)} + f_0^{(1)} + \dots, \quad (36)$$

where the approximation $f_0^{(k)}$ is of order k in the spatial gradients. The implementation of the Chapman–Enskog method to first order in the spatial gradients follows similar steps as those made in the conventional IHS model.^{30,35–37} Here, only the final results for the integral equations verifying the diffusion transport coefficients will be displayed.

The first-order distribution function $f_0^{(1)}(\mathbf{V})$ is given by

$$\begin{aligned}f_0^{(1)} = & \mathbf{A}_0 \cdot \nabla n_0 + \mathbf{B}_0 \cdot \nabla n + \mathbf{C}_0 \cdot \nabla T + \mathcal{D}_{0,ij} \nabla_i U_j \\ & + \mathcal{E}_0 \nabla \cdot \mathbf{U},\end{aligned}\quad (37)$$

where an implicit summation over repeated indices is used in Eq. (37). The quantities $\mathbf{A}_0(\mathbf{V})$, $\mathbf{B}_0(\mathbf{V})$, $\mathbf{C}_0(\mathbf{V})$, $\mathcal{D}_{0,ij}(\mathbf{V})$, and $\mathcal{E}_0(\mathbf{V})$ obey certain integral equations. Since we are interested here in obtaining the diffusion transport coefficients, we will only pay attention to the unknowns $\mathbf{A}_0(\mathbf{V})$, $\mathbf{B}_0(\mathbf{V})$, and $\mathbf{C}_0(\mathbf{V})$ (this is equivalent to assume a nonequilibrium state with vanishing flow velocity).

The first-order contribution $\mathbf{j}_0^{(1)}$ to the mass flux is given by Eq. (1). In terms of \mathbf{A}_0 , \mathbf{B}_0 , and \mathbf{C}_0 , the diffusion transport coefficients D_T , D_0 , and D are defined,

respectively, as

$$D_T = -\frac{m_0}{\rho d} \int d\mathbf{v} \mathbf{V} \cdot \mathbf{A}_0(\mathbf{V}). \quad (38)$$

$$D_0 = -\frac{\rho}{m_0 n_0 d} \int d\mathbf{v} \mathbf{v} \cdot \mathbf{B}_0(\mathbf{V}), \quad (39)$$

$$D = -\frac{1}{d} \int d\mathbf{v} \mathbf{V} \cdot \mathbf{C}_0(\mathbf{V}), \quad (40)$$

The unknowns $\mathbf{A}_0(\mathbf{V})$, $\mathbf{B}_0(\mathbf{V})$, and $\mathbf{C}_0(\mathbf{V})$ are the solutions of the following set of coupled linear integral equations:

$$\begin{aligned}-\zeta^{(0)} T \partial_T \mathbf{A}_0 - \frac{1}{2} \zeta^{(0)} \left(1 - \Delta^* \frac{\partial \ln \zeta^*}{\partial \Delta^*}\right) \mathbf{A}_0 - J_0^{(0)} [\mathbf{A}_0, f^{(0)}] \\ = \mathbf{A}_0 + J_0^{(0)} [f_0^{(0)}, \mathbf{A}],\end{aligned}\quad (41)$$

$$-\zeta^{(0)} T \partial_T \mathbf{B}_0 - J_0^{(0)} [\mathbf{B}_0, f^{(0)}] = \mathbf{B}_0, \quad (42)$$

$$\begin{aligned}-\zeta^{(0)} T \partial_T \mathbf{C}_0 - J_0^{(0)} [\mathbf{C}_0, f^{(0)}] = \mathbf{C}_0 + \zeta^{(0)} \left(1 + \phi \frac{\partial \ln \chi}{\partial \phi}\right) \\ \times \mathbf{A}_0 + J_0^{(0)} [f_0^{(0)}, \mathbf{C}].\end{aligned}\quad (43)$$

In Eqs. (41)–(43), $\zeta^{(0)}$ is the zeroth-order contribution to ζ and $\zeta^* = \zeta^{(0)}/\nu$. An explicit (but approximate) form of the cooling rate $\zeta^{(0)}$ is given by Eq. (19). In addition, the coefficients \mathbf{A}_0 , \mathbf{B}_0 , and \mathbf{C}_0 are given, respectively, by

$$\begin{aligned}\mathbf{A}_0(\mathbf{V}) = & -\mathbf{V} T \frac{\partial f_0^{(0)}}{\partial T} - \frac{p}{\rho} \left(1 - \frac{1}{2} \Delta^* \frac{\partial \ln p^*}{\partial \Delta^*}\right) \frac{\partial f_0^{(0)}}{\partial \mathbf{V}} \\ & - \mathcal{K}_0 \left[T \frac{\partial f_0^{(0)}}{\partial T}\right],\end{aligned}\quad (44)$$

$$\mathbf{B}_0(\mathbf{V}) = -\mathbf{V} n_0 \frac{\partial f_0^{(0)}}{\partial n_0}, \quad (45)$$

$$\begin{aligned}\mathbf{C}_0(\mathbf{V}) = & -\mathbf{V} n \frac{\partial f_0^{(0)}}{\partial n} - m^{-1} \frac{\partial p}{\partial n} \frac{\partial f_0^{(0)}}{\partial \mathbf{V}} \\ & - \frac{(1+\omega)^{-d}}{\chi_0 T} \left(\frac{\partial \mu_0}{\partial \phi}\right)_{T, n_0} \mathcal{K}_0 [f^{(0)}].\end{aligned}\quad (46)$$

Here, $\omega = \sigma_0/\sigma$ is the diameter ratio, μ_0 is the chemical potential of the intruder, and the operator $\mathcal{K}_0[X]$ is defined as

$$\begin{aligned} \mathcal{K}_0[X] = & -\bar{\sigma}^d \chi_0 \int d\mathbf{v}_2 \int d\hat{\boldsymbol{\sigma}} \Theta(-\hat{\boldsymbol{\sigma}} \cdot \mathbf{g}_{12} - 2\Delta_0)(-\hat{\boldsymbol{\sigma}} \cdot \mathbf{g}_{12} - 2\Delta_0) \hat{\boldsymbol{\sigma}} \alpha_0^{-2} f_0^{(0)}(\mathbf{V}_1'') X(\mathbf{V}_2'') \\ & + \bar{\sigma}^d \chi_0 \int d\mathbf{v}_2 \int d\hat{\boldsymbol{\sigma}} \Theta(\hat{\boldsymbol{\sigma}} \cdot \mathbf{g}_{12})(\hat{\boldsymbol{\sigma}} \cdot \mathbf{g}_{12}) \hat{\boldsymbol{\sigma}} f_0^{(0)}(\mathbf{V}_1) X(\mathbf{V}_2). \end{aligned} \quad (47)$$

In addition,

$$\begin{aligned} J_0^{(0)}[f_0^{(0)}, X] = & \bar{\sigma}^{d-1} \chi_0 \int d\mathbf{v}_2 \int d\hat{\boldsymbol{\sigma}} \Theta(-\hat{\boldsymbol{\sigma}} \cdot \mathbf{g}_{12} - 2\Delta_0)(-\hat{\boldsymbol{\sigma}} \cdot \mathbf{g}_{12} - 2\Delta_0) \alpha_0^{-2} f_0^{(0)}(\mathbf{V}_1'') X(\mathbf{V}_2'') \\ & - \bar{\sigma}^{d-1} \chi_0 \int d\mathbf{v}_2 \int d\hat{\boldsymbol{\sigma}} \Theta(\hat{\boldsymbol{\sigma}} \cdot \mathbf{g}_{12})(\hat{\boldsymbol{\sigma}} \cdot \mathbf{g}_{12}) f_0^{(0)}(\mathbf{V}_1) X(\mathbf{V}_2), \end{aligned} \quad (48)$$

and we have accounted for that the first-order distribution $f^{(1)}(\mathbf{V})$ of the granular gas is given by

$$f^{(1)}(\mathbf{V}) = \mathcal{A}(\mathbf{V}) \cdot \nabla \ln T + \mathcal{C}(\mathbf{V}) \cdot \nabla \ln n + \mathcal{D}_{ij}(\mathbf{V}) \nabla_i U_j + E(\mathbf{V}) \nabla \cdot \mathbf{U}, \quad (49)$$

where the quantities \mathcal{A} , \mathcal{C} , \mathcal{D}_{ij} and E obey a set of coupled linear integral equations.³⁸

As for elastic collisions,²⁴ to get explicit expressions for the diffusion transport coefficients one considers the leading terms in a Sonine polynomial expansion of the unknowns \mathcal{A}_0 , \mathcal{B}_0 , and \mathcal{C}_0 . This task is carried out in Sec. V.

V. FIRST-SONINE APPROXIMATION TO THE DIFFUSION TRANSPORT COEFFICIENTS AT THE STATIONARY TEMPERATURE

The lowest order Sonine polynomial approximations for $\mathcal{A}_0(\mathbf{V})$, $\mathcal{B}_0(\mathbf{V})$, and $\mathcal{C}_0(\mathbf{V})$ are

$$\mathcal{A}_0(\mathbf{V}) \rightarrow -f_{0,M}(\mathbf{V}) \frac{\rho}{n_0 T_0^{(0)}} \mathbf{V} D_T, \quad (50)$$

$$\mathcal{B}_0(\mathbf{V}) \rightarrow -f_{0,M}(\mathbf{V}) \frac{m_0^2}{\rho T_0^{(0)}} \mathbf{V} D_0, \quad (51)$$

$$\mathcal{C}_0(\mathbf{V}) \rightarrow -f_{0,M}(\mathbf{V}) \frac{m_0}{n_0 T_0^{(0)}} \mathbf{V} D, \quad (52)$$

where $T_0^{(0)}$ is the zeroth-order contribution to the partial temperature T_0 and the Maxwellian distribution $f_{0,M}(\mathbf{V})$ is given by Eq. (34) with the replacements $\mathbf{v} \rightarrow \mathbf{V}$ and $T_0 \rightarrow T_0^{(0)}$. Moreover, in the lowest Sonine approximation, $\mathcal{A} = \mathcal{C} = \mathbf{0}$, and then the impurities do not inherit any contribution coming from the granular gas. The transport coefficients D_0 , D , and D_T are determined by substitution of Eqs. (50)–(52) into the integral equations (41)–(43), multiplication of them by $m_0 \mathbf{V}$ and integration over velocity. Some technical details on this calculation are displayed in the Appendix A. Here, we provide the final expressions for the coefficients D_0 , D , and D_T in the relevant state of a two-dimensional confined granular mixture with stationary temperature. In this case, $\zeta^{(0)} = \zeta_0^{(0)} = 0$ and the differential equations (A3),

(A10), and (A12) obeying the diffusion coefficients (in dimensionless form) become linear algebraic equations.

The expressions of the diffusion transport coefficients D_0 , D_T , and D in the steady state are given, respectively, by

$$D_0 = \frac{\rho T}{m_0^2 \nu} \frac{\gamma_0}{\nu_D^*}, \quad (53)$$

$$D_T = \frac{n_0 T}{\rho \nu} \frac{X_0^*}{\nu_D^* + \frac{1}{2} \Delta^* \frac{\partial \zeta^*}{\partial \Delta^*}}, \quad (54)$$

$$D = \frac{n_0 T}{m_0 \nu} \frac{Y_0^*}{\nu_D^*}. \quad (55)$$

In Eqs. (53)–(55), the dimensionless quantities ν_D^* , X_0^* , and Y_0^* are given, respectively, by

$$\nu_D^* = \frac{2\pi^{\frac{d-1}{2}}}{d\Gamma\left(\frac{d}{2}\right)} \chi_0 \left(\frac{\bar{\sigma}}{\sigma}\right)^{d-1} M \left[\left(\frac{1+\theta}{\theta}\right)^{1/2} (1+\alpha_0) + \sqrt{\pi} \Delta_0^* \right], \quad (56)$$

$$\begin{aligned} X_0^* = & \gamma_0 \left(1 - \frac{1}{2} \tilde{\Delta}^* \frac{\partial \ln \gamma_0}{\partial \tilde{\Delta}^*}\right) - \mu \left(p^* - \frac{2^{d-1}}{\sqrt{2\pi}} \chi \phi \Delta^*\right) \\ & + 2^d \left(\frac{\bar{\sigma}}{\sigma}\right)^d \phi \chi_0 M_0 \left[\frac{1+\alpha_0}{2} + \frac{\Delta_0^*}{\sqrt{\pi}} \left(\frac{\theta}{1+\theta}\right)^{1/2} \right], \end{aligned} \quad (57)$$

$$\begin{aligned} Y_0^* = & -\mu \left(p^* + \phi \frac{\partial p^*}{\partial \phi}\right) + \phi M_0 \left(\frac{\partial \mu_0/T}{\partial \phi}\right)_T \left(\frac{1+\theta}{\theta}\right) \\ & \times \left[\frac{1+\alpha_0}{2} + \frac{2\Delta_0^*}{\sqrt{\pi}} \left(\frac{\theta}{1+\theta}\right)^{1/2} \right], \end{aligned} \quad (58)$$

where $\gamma_0 = T_0^{(0)}/T$, $\mu = m_0/m$ is the mass ratio, and we have introduced the shorthand notation

$$\tilde{\Delta}^* \frac{\partial}{\partial \tilde{\Delta}^*} \equiv \Delta^* \frac{\partial}{\partial \Delta^*} + \Delta_0^* \frac{\partial}{\partial \Delta_0^*}. \quad (59)$$

Note that in the particular case $\Delta^* = \Delta_0^*$, only one of the two terms of the identity (59) must be considered. The evaluation of the derivative $\tilde{\Delta}^* \partial_{\tilde{\Delta}^*}$ appearing in Eq. (57) is performed in the Appendix A.

In order to get the explicit dependence of the transport coefficients on the parameter space of the system, one has to give the forms of the pair correlation functions χ and χ_0 . In the case of a two-dimensional system ($d = 2$), a good approximation for χ is³⁹

$$\chi = \frac{1 - \frac{7}{16}\phi}{(1 - \phi)^2}, \quad (60)$$

while the intruder-gas pair correlation function is given by

$$\chi_0 = \frac{1}{1 - \phi} + \frac{9}{8} \frac{\omega}{1 + \omega} \frac{\phi}{(1 - \phi)^2}. \quad (61)$$

The expression for the chemical potential of the impurities consistent with the approximation (61) is

$$\begin{aligned} \frac{\mu_0}{T} = & \ln(\lambda_0^2 n_0) + \ln n_0 - \ln(1 - \phi) \\ & + \frac{1}{4}\omega \left[\frac{9\phi}{1 - \phi} + \ln(1 - \phi) \right] \\ & - \frac{\omega^2}{8} \left[\frac{\phi(1 - 10\phi)}{(1 - \phi)^2} - \frac{8\phi}{1 - \phi} + \ln(1 - \phi) \right], \end{aligned} \quad (62)$$

where $\lambda_0(T)$ is the (constant) de Broglie's thermal wavelength.⁴⁰

Before considering some illustrative systems to assess the dependence of the diffusion coefficients on the parameter space of the system, it is quite instructive to pay attention to some limiting cases.

A. Mechanically equivalent particles

For mechanically equivalent particles ($m = m_0$, $\sigma = \sigma_0$, $\alpha = \alpha_0$, and $\Delta = \Delta_0$), it is easy to see that $X_0^* = 0$ and $Y_0^* = -1$. In this case, $D_T = 0$ and $D = -(n_0/n)D_0$, as expected. The mass flux \mathbf{j}_0 obeys the constitutive equation

$$\mathbf{j}_0 = -mD_0 \nabla x_0, \quad (63)$$

where

$$D_0 = \frac{d\Gamma\left(\frac{d}{2}\right)}{2\pi^{(d-1)/2}} \frac{\sigma^{1-d}}{\chi} \sqrt{\frac{T}{m}} \left(1 + \alpha + \sqrt{\frac{\pi}{2}} \Delta^*\right)^{-1} \quad (64)$$

is the self-diffusion coefficient.

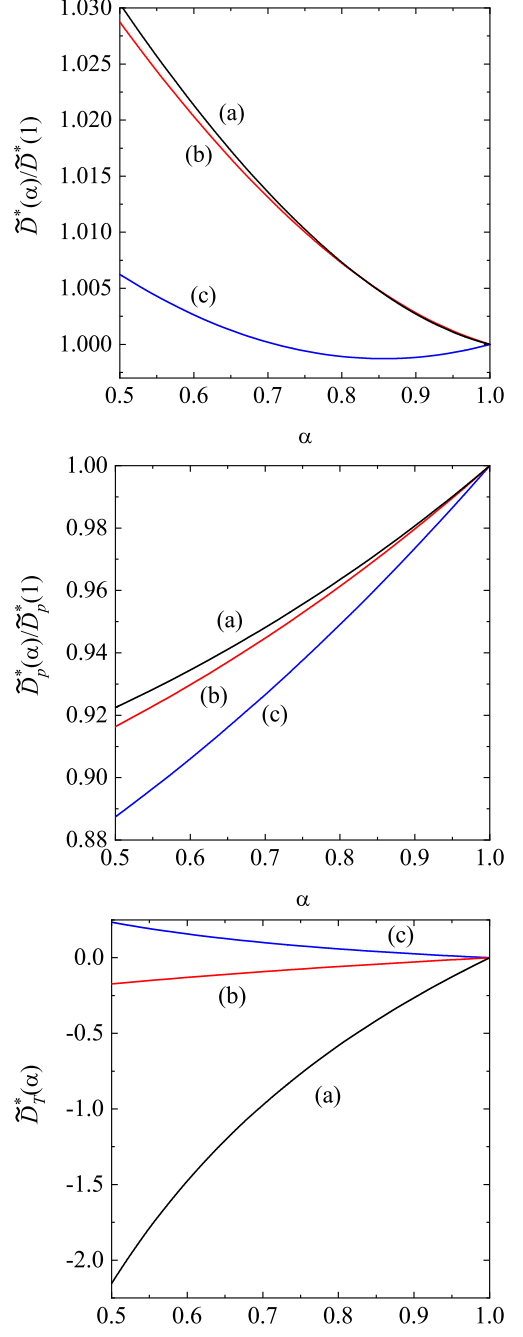


FIG. 1. Plot of the (dimensionless) diffusion coefficients $\tilde{D}^*(\alpha)/\tilde{D}^*(1)$, $\tilde{D}_p^*(\alpha)/\tilde{D}_p^*(1)$, and $\tilde{D}_T^*(\alpha)$ vs the (common) coefficient of restitution $\alpha = \alpha_0$ for $d = 2$, $\phi = 0$, and three different binary mixtures: $\sigma_0/\sigma = 2$, $m_0/m = 4$ (a); $\sigma_0/\sigma = 2$, $m_0/m = 2$ (b); and $\sigma_0/\sigma = 0.2$, $m_0/m = 0.8$ (c). Here, $\Delta^* = \Delta_0^*$ and $\tilde{D}^*(1)$ and $\tilde{D}_p^*(1)$ refer to the values of the diffusion coefficients for elastic collisions ($\alpha = 1$).

B. Low-density limit

Let us consider now the low-density limit ($\phi \rightarrow 0$). In this case, to compare with the results derived in Ref. 21 for general concentration (or mole fraction) $x_0 \equiv n_0/n$, it is convenient to express the constitutive equation (1) in terms of the spatial gradients of x_0 , $p = nT$ and T . In this representation,

$$\mathbf{j}_0^{(1)} = -\frac{mm_0n}{\rho} \tilde{D} \nabla x_0 - \frac{\rho}{p} \tilde{D}_p \nabla p - \frac{\rho}{T} \tilde{D}_T \nabla T, \quad (65)$$

where the relationship between the diffusion coefficients $\{\tilde{D}, \tilde{D}_p, \tilde{D}_T\}$ and $\{D_0, D, D_T\}$ is

$$D_0 = \mu^{-1} \tilde{D}, \quad D = \frac{\rho}{m_0} \tilde{D}_p - x_0 \tilde{D}, \quad D_T = \tilde{D}_p + \tilde{D}_T. \quad (66)$$

In the dilute limit ($\phi \rightarrow 0$), Eqs. (53)–(55) for the coefficients D_0 , D_T , and D reduce to

$$D_0 = \frac{\rho T}{m_0^2 \nu} \frac{\gamma_0}{\nu_D^*}, \quad D = -\frac{n_0 T}{m_0 \nu} \frac{\mu}{\nu_D^*}, \quad (67)$$

$$D_T = \frac{n_0 T}{\rho \nu} \frac{\gamma_0 \left(1 - \frac{1}{2} \Delta^* \frac{\partial \ln \gamma_0}{\partial \Delta^*}\right) - \mu}{\nu_D^* + \frac{1}{2} \Delta^* \frac{\partial \zeta^*}{\partial \Delta^*}}, \quad (68)$$

where ν_D^* is given by Eq. (56) with $\chi_0 = 1$. Substitution of Eqs. (67) and (68) into the relationships (66) yield

$$\tilde{D} = \frac{\rho T}{mm_0 \nu} \frac{\gamma_0}{\nu_D^*}, \quad (69)$$

$$\tilde{D}_p = x_0 \frac{n T}{\rho \nu} \frac{\gamma_0 - \mu}{\nu_D^*}, \quad (70)$$

$$\tilde{D}_T = -x_0 \frac{n T}{\rho \nu} \frac{\Delta^* \frac{\partial \gamma_0}{\partial \Delta^*} + \Delta^* \frac{\partial \zeta^*}{\partial \Delta^*} \tilde{D}_p^*}{2\nu_D^* + \Delta^* \frac{\partial \zeta^*}{\partial \Delta^*}}, \quad (71)$$

where $\tilde{D}_p^* = (\rho \nu / x_0 n T) \tilde{D}_p$. Equations (69)–(71) are consistent with those obtained for dilute granular mixtures in the tracer limit ($x_0 \rightarrow 0$).²¹

The dependence of the (dimensionless) diffusion transport coefficients $\tilde{D}^*(\alpha)/\tilde{D}^*(1)$, $\tilde{D}_p^*(\alpha)/\tilde{D}_p^*(1)$, and $\tilde{D}_T^*(\alpha)$ on a (common) coefficient of restitution $\alpha = \alpha_0$ is plotted in Fig. 1 for three different two-dimensional ($d = 2$) mixtures. Here, $\Delta^* = \Delta_0^*$, $\tilde{D}^* = (mm_0 \nu / \rho T) \tilde{D}$, and $\tilde{D}_T^* = (\rho \nu / x_0 n T) \tilde{D}_T$. Moreover, $\tilde{D}^*(1)$ and $\tilde{D}_p^*(1)$ refer to the values of the diffusion coefficients for elastic collisions ($\alpha = 1$). The (dimensionless) thermal diffusion coefficient \tilde{D}_T^* has not been reduced with its elastic value because this coefficient vanishes when $\alpha = 1$ for dilute gases in the first Sonine approximation.^{24,41} As already noted in previous works,²¹ Fig. 1 shows that the impact of inelasticity on the diffusion coefficients is in

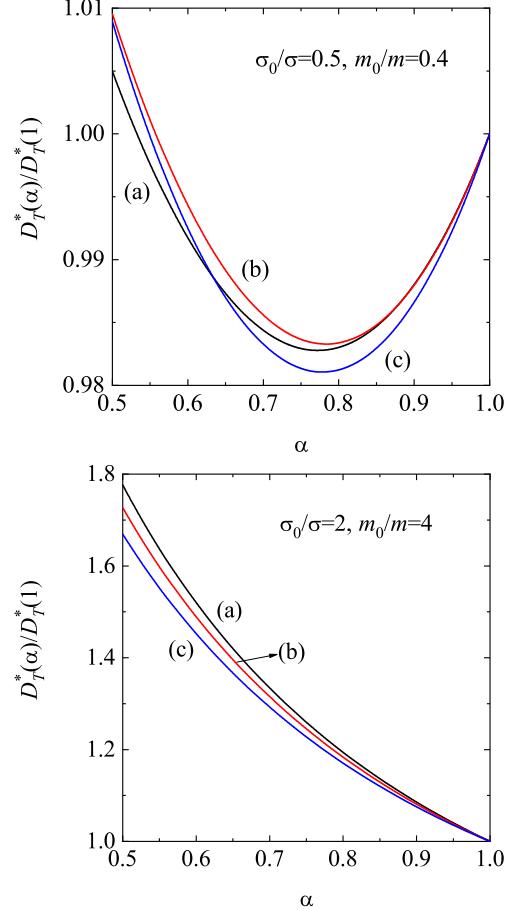


FIG. 2. Plot of the (dimensionless) transport diffusion coefficient $D_T^*(\alpha)/D_T^*(1)$ vs the (common) coefficient of restitution $\alpha = \alpha_0$ for $d = 2$, two different binary mixtures ($\sigma_0/\sigma = 2$, $m_0/m = 4$ and $\sigma_0/\sigma = 0.5$, $m_0/m = 0.4$) and three different values of the solid volume fraction ϕ : $\phi = 0$ (a), $\phi = 0.1$ (b), and $\phi = 0.2$ (c). Here, $\Delta^* = \Delta_0^*$ and $D_T^*(1)$ refers to the value of D_T^* for elastic collisions ($\alpha = 1$).

general smaller than the one found in the conventional IHS model.⁴² Regarding the tracer diffusion coefficient \tilde{D}^* , we see this coefficient increases with respect to its elastic value as the inelasticity increases, except when the intruder is smaller and/or lighter than the granular gas particles; there exists a small region around $\alpha = 1$ where the scaled coefficient $\tilde{D}^*(\alpha)/\tilde{D}^*(1)$ exhibits a non-monotonic dependence on inelasticity. In the case of the (scaled) coefficient $\tilde{D}_p^*(\alpha)/\tilde{D}_p^*(1)$ we observe that it decreases with decreasing α (regardless of the value of the diameter and/or mass ratio while the thermal diffusion coefficient $\tilde{D}_T^*(\alpha)$ can be positive or negative depending on the system considered. This behavior agrees qualitatively to what happens in the IHS model.²¹ As will show later, the signature of the coefficient $\tilde{D}_T^*(\alpha)$ is important in segregation problems induced by a thermal gradient.^{31,43–50}

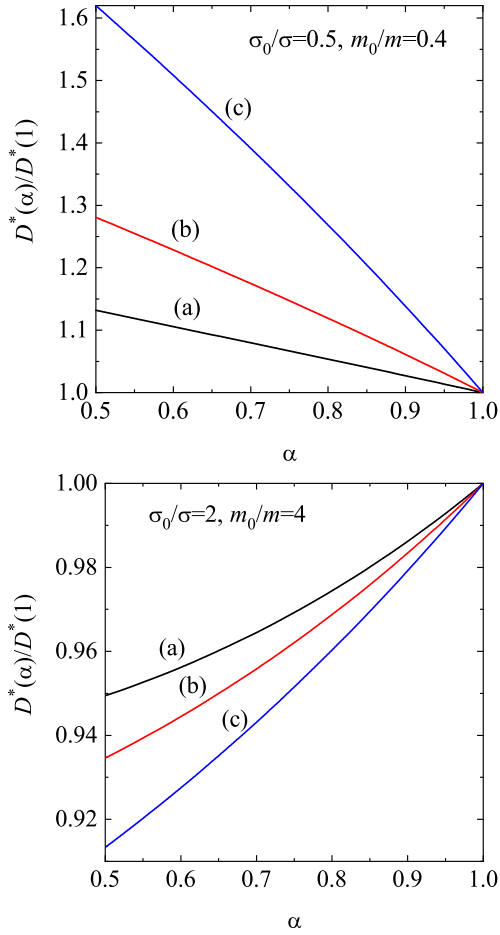


FIG. 3. Plot of the (dimensionless) transport diffusion coefficient $D^*(\alpha)/D^*(1)$ vs the (common) coefficient of restitution $\alpha = \alpha_0$ for $d = 2$, two different binary mixtures ($\sigma_0/\sigma = 2$, $m_0/m = 4$ and $\sigma_0/\sigma = 2$, $m_0/m = 0.4$) and three different values of the solid volume fraction ϕ : $\phi = 0$ (a), $\phi = 0.1$ (b), and $\phi = 0.2$ (c). Here, $\Delta^* = \Delta_0^*$ and $D^*(1)$ refers to the value of D^* for elastic collisions ($\alpha = 1$).

C. Some illustrative systems for moderate densities

Now, we want to assess the dependence of the (scaled) diffusion coefficients on the parameter space of the system for a two-dimensional system. The parameter space is constituted by the diameter σ_0/σ and mass m_0/m ratios, the coefficients of restitution α and α_0 , the solid volume fraction ϕ , and the (dimensionless) parameters associated with the energy injection at collisions Δ^* and $\Delta_0^* = \lambda\Delta^*$ ($\lambda \geq 0$). The parameter λ is therefore a measure in the contrast of energy injection at tracer-gas collisions compared to gas-gas collisions. Since we are mainly interested on the influence of both inelasticity and density on mass transport, we first analyze the usual case for binary mixtures, that is, when the components differ only in their masses and diameters. Hence, we assume here that $\alpha = \alpha_0$ and $\lambda = 1$. In addition, because in

the steady state Δ^* is only a function of α [see Eq. (20)], then the parameter space is reduced to three parameters $\{\sigma_0/\sigma, m_0/m, \alpha\}$.

According to Eq. (53), the (dimensionless) tracer diffusion coefficient $D_0^* = (m_0^2 \nu / \rho T) D_0$ is given by

$$D_0^* = \frac{\gamma_0}{\chi_0 \nu_D^*}. \quad (72)$$

Since the temperature ratio γ_0 is obtained from the condition $\zeta_0 = 0$, then it is independent of the density ϕ . Consequently, according to Eq. (56), the scaled coefficient $D_0^*(\alpha)/D_0^*(1)$ is independent of the density and hence, its dependence on α is the same as that of a dilute gas (see Fig. 1). For this reason, we focus our attention now in the scaled coefficients $D_T^*(\alpha)/D_T^*(1)$ and $D^*(\alpha)/D^*(1)$, where $D_T^* = (\rho \nu / n_0 T) D_T$ and $D^* = (m_0 \nu / n_0 T) D$. As said before, $D_T^*(1)$ and $D^*(1)$ refer to the values of D_T^* and D^* , respectively, for elastic collisions ($\alpha = 1$). According to Eq. (57), note that for dense gases $X_0^* \neq 0$ and so, $D_T^*(1) \neq 0$ when $\phi \neq 0$.

Figure 2 shows the dependence of the ratio $D_T^*(\alpha)/D_T^*(1)$ on α for three different values of the density ϕ . Two different mixtures are considered. We observe first that while this scaled coefficient exhibits a non-monotonic dependence on inelasticity when both mass and diameter ratios are smaller than 1, $D_T^*(\alpha)/D_T^*(1)$ increases with increasing inelasticity when the intruder is heavier and/or larger than the particles of the granular gas. This behavior contrasts with the one found in the conventional IHS (see the lines of the first Sonine solution of Fig. 3 in Ref. 30). With respect to the influence of density, at a given value of α , we see in general a weak effect of ϕ on the (scaled) thermal diffusion coefficient. To complement this figure, the (scaled) coefficient $D^*(\alpha)/D^*(1)$ is plotted in Fig. 3 as a function of α for the same systems as those considered in Fig. 2. In contrast to D_T^* , stronger influence of density on $D^*(\alpha)/D^*(1)$ is observed. At a given value of α , while this scaled coefficient increases as the granular gas becomes denser when $m_0 > m$ and $\sigma_0 > \sigma$, the opposite happens when the impurity is lighter and/or smaller than the particles of the granular gas. As in the case of D_T^* , a comparison with the results obtained in the IHS model (see the lines of the first Sonine solution of Fig. 2 in Ref. 30) shows again a completely different qualitative behavior. As a general conclusion, our results clearly show that the impact of inelasticity on mass transport for a confined system (modeled via the Δ model) is less significant than the one observed in freely cooling systems. This is the expected result based on the previous work²¹ on dilute granular mixtures.

VI. COMPARISON WITH COMPUTER SIMULATIONS

The theoretical results derived for the diffusion transport coefficients are based on a relatively crude approximation: they have been obtained by considering the

leading term in a Sonine polynomial expansion. Thus, it seems convenient to assess the accuracy of the above theoretical results by comparing them with computer simulations. Here, we compare the expression (53) for the tracer diffusion coefficient D_0 with both numerical results obtained from the DSMC method²⁸ and from MD simulations.^{25–27} In this case, we consider the diffusion of tracer particles in a granular gas of mechanically different particles in the HSS. In this situation, $\nabla \mathbf{U} = \mathbf{0}$, $\nabla n = \nabla T = 0$ and so, the constitutive equation (37) can be written as

$$\mathbf{j}_0^{(1)} = -\frac{m_0^2 n}{\rho} D_0 \nabla x_0, \quad (73)$$

where we recall that $x_0 = n_0/n$. Then, the balance equation (31) for the concentration becomes

$$\frac{\partial x_0}{\partial t} = \frac{m_0 D_0}{\rho} \nabla^2 x_0. \quad (74)$$

Equation (74) is the standard diffusion equation with the time-independent diffusion coefficient $D_{\text{tracer}} = m_0 D_0 / \rho$. In simulations, we can obtain the Mean Square Displacement (MSD) of the tracer particles after a time interval t as

$$\text{MSD}(t) = \langle |\mathbf{r}(t) - \mathbf{r}(0)|^2 \rangle, \quad (75)$$

where $|\mathbf{r}(t) - \mathbf{r}(0)|$ is the distance travelled by the tracer particles from $t = 0$ until the instant t . From it, the Einstein relation gives

$$D_{\text{tracer}} = \frac{1}{2d} \frac{d \text{MSD}(t)}{dt}. \quad (76)$$

Equation (76) finally permits us to obtain the diffusion coefficient D_0 .

The DSMC method is a direct particle numerical method to find solutions to the Boltzmann²⁸ and Enskog^{51,52} kinetic equations, without the need of considering uncontrolled approximations such as the truncation of a Sonine polynomial expansion. Thus, in the limit of an infinitely large number of particles and small time step, the DSMC method provides the “exact” solution of the kinetic equation. It is therefore an excellent method to assess the reliability of the theoretical expression (53) for D_0 obtained from the first Sonine approximation. In practice, we consider $N = 4000$ particles, one of which is the tracer particle, simulated in homogeneous conditions. This means that no spatial grid is constructed during the simulations and particles can collide with all of them. Collisions, which are sampled statistically, are performed following the collision rules (2)–(3) and (27)–(28). Since the granular gas is in the HSS, the influence of the gas density $n\sigma^d$ on diffusion in the DSMC method enters only in fixing the collision rate. Thus, as in the Enskog theory, the density dependence in the DSMC method appears through the pair correlation factors at contact χ and χ_0 given by Eqs. (60) and (61), respectively. Finally, the

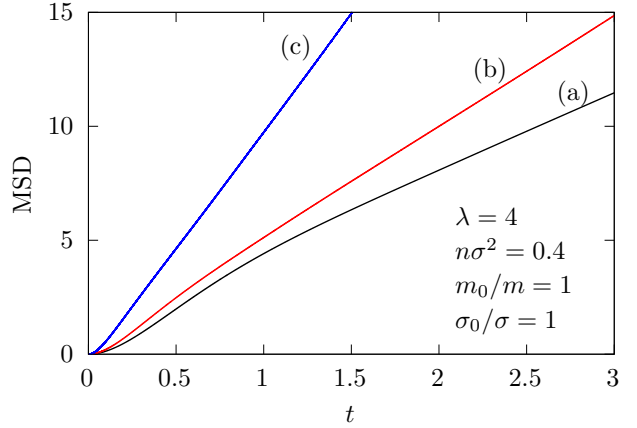


FIG. 4. Mean-square displacements for tracer particles obtained in MD. The simulation parameters are $n\sigma^2 = 0.4$, $\lambda \equiv \Delta_0/\Delta = 4$, and $\sigma_0/\sigma = m_0/m = 1$, with a common coefficient of restitution $\alpha = \alpha_0 = 0.2$ (a), 0.5 (b), and 0.8 (c).

time step is set equal to one fiftieth of the mean collision time in the gas.

Molecular dynamics can be considered as an exact numerical solution of the particle dynamics, following the collision rules (2)–(3) and (27)–(28). As such, it makes no assumptions of molecular chaos, homogeneity, or normal solutions. Its results allow us to put strong tests on the hypothesis behind the kinetic description made in this article. For MD, we consider $N = 4000$ particles, one of them being the tracer, which are simulated using the event-driven method^{25–27} in a square box with periodic boundary conditions, and a box size adjusted to give the desired particle density. Both in DSMC and MD, large simulations are done to obtain convergence of the MSD.

A. Regimes in the mean-square displacement

Figure 4 shows typical MSD curves obtained with MD simulations. It is evident a first ballistic regime, lasting for a time of the order of the mean collision time. At long times, a diffusive regime appears, which allows us to obtain the diffusion coefficient using Einstein’s relation (76). In cases of high density and small coefficients of restitution, three instead of two regimes appear (see, for example, the curves (a) and (b) in Fig. 4). First, there is the usual ballistic regime. It is followed by an intermediate diffusive regime with a diffusion coefficient $D_{\text{transient}}$ and, later, a second and definitive diffusive regime is established with a smaller diffusion coefficient D_{tracer} . The measurements presented in this paper are obtained in the last regime.

In the case of the DSMC method, only the ballistic and diffusion regimes are obtained (not shown). This implies that the origin of this anomalous behavior in MD can only be due to correlations neglected in the kinetic de-

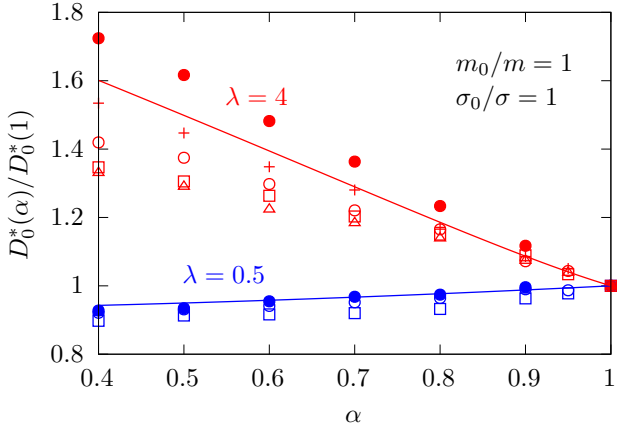


FIG. 5. Comparison with simulations: case I. Normalized diffusion coefficient $D_0^*(\alpha)/D_0^*(1)$ as a function of the (common) coefficient of restitution $\alpha = \alpha_0$ for a tracer particle of equal mass and diameter of the particles of the granular gas, but with $\Delta_0 = \lambda\Delta$, with $\lambda = 0.5$ (blue) and 4.0 (red). Theory in solid lines, DSMC results with solid circles, and MD simulations with open symbols ($n\sigma^2 = 0.05$, crosses; $n\sigma^2 = 0.1$, circles; $n\sigma^2 = 0.2$, triangles; and $n\sigma^2 = 0.4$, squares).

scription. Specifically, as in Fig. 4, the value of $\lambda = 4$ is chosen and hence the tracer-particle collision is characterized by a large value of Δ . Therefore, the tracer particle acts as a local energy source, which is lately dissipated in the granular gas. As a result, the granular gas is driven into a *inhomogeneous* state, hotter and more dilute near the tracer. This changes the local environment for the tracer particle, which can diffuse faster in this cloud, resulting in this larger value of $D_{\text{transient}}$. At longer times, the tracer itself must move the cloud, and the diffusion of the dressed object is described by the long term diffusion coefficient D_{tracer} . The analysis of this dynamical process is beyond the scope of this manuscript and is left to future work. Nevertheless, we would like to note that, despite its complexity, the numerical values obtained in MD for D_{tracer} in general have a good quantitative agreement (except for a rather strong inelasticity) with the simple kinetic-theoretical prediction of D_0 given by the expression (53) (see especially figures 5 and 6 in the following section).

B. Diffusion coefficients

We consider three different cases for study. In case I, the tracer particle has equal mass, diameter, and coefficient of restitution as the particles of the granular gas; it differs in the energy injection at collisions, with $\Delta_0 = \lambda\Delta$. Figure 5 presents the diffusion coefficient normalized to the elastic case $D_0^*(\alpha)/D_0^*(1)$ as a function of α for $\lambda = 0.5$ and 4. The theory predicts that the result is independent of density, result that is trivially obtained in DSMC because by construction of the method, the col-

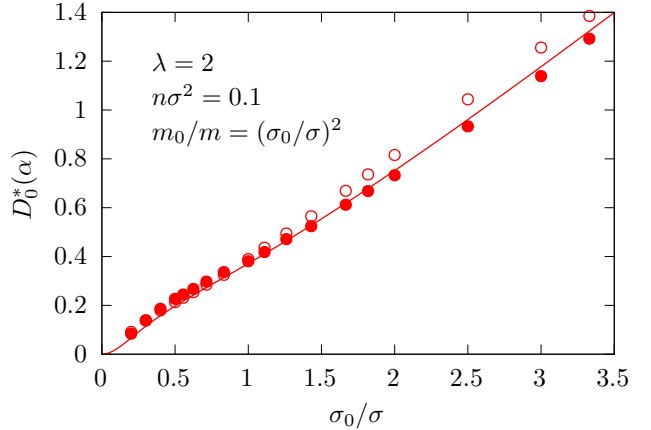


FIG. 6. Comparison with simulations: case II. Diffusion coefficient $D_0^*(\alpha)$ as a function of the diameter ratio σ_0/σ for a tracer particle with the same mass density as the particles of the granular gas [$m_0/m = (\sigma_0/\sigma)^2$]. The (common) coefficient of restitution is $\alpha = \alpha_0 = 0.8$, the contrast parameter $\lambda \equiv \Delta_0/\Delta = 2$, and the (reduced) density $n\sigma^2 = 0.1$. Theory in solid lines, MD simulations with open circles, and DSMC results with solid circles.

lision frequency scales out when the normalized diffusion coefficient is plotted. As a consequence, only one density (with a value that is immaterial) is used for DSMC. In the case of MD simulations, several densities are used and there is an appreciable dependence with this parameter. We observe that the normalized diffusion coefficient decreases with increasing density, especially for the case of large contrast ($\lambda = 4$). The DSMC results show good agreement with theory, with deviations increasing for more inelastic conditions. This is expected as the theoretical prediction has been obtained considering up to the first Sonine approximation and DSMC results can be considered an “exact” solution of the kinetic equation. As expected from previous works^{29,30} for tracer diffusion in the IHS model, going to larger inelasticities would require using more higher order approximations to achieve more accurate predictions. Regarding the MD simulations, the agreement is also good, except for the large contrast case, with large inelasticities and high densities. The deviations in these cases (which go in the opposite direction of the DSMC results) are essentially due to correlations not accounted for in the Enskog kinetic theory description. These include velocity correlations between the particles which are about to collide (breakdown of the molecular chaos hypothesis) and the spatial inhomogeneities described in Sec. VI A. The effect of both on diffusion increases with the contrast parameter λ , inelasticities, and density.

The case II considers tracers of different mass and radius compared to the particles of the granular gas, but still having the same mass density (i.e., $m_0/\sigma_0^2 = m/\sigma^2$). In Fig. 6, we present the diffusion coefficient $D_0^*(\alpha)$ as a function of the diameter ratio σ_0/σ for $\lambda = 2$, a (com-

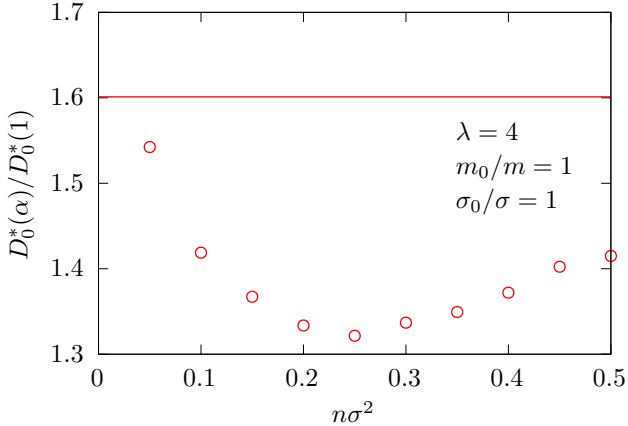


FIG. 7. Comparison with MD simulations: case III. Normalized diffusion coefficient $D_0^*(\alpha)/D_0^*(1)$ as a function of the (reduced) density $n\sigma^2$ of the granular gas, for a tracer particle of equal mass and diameter of the particles of the granular gas. The (common) coefficient of restitution is $\alpha = \alpha_0 = 0.4$ and $\lambda \equiv \Delta_0/\Delta = 4$. Theory in a solid line and MD results with open circles.

mon) coefficient of restitution $\alpha = \alpha_0 = 0.8$, and a (reduced) density $n\sigma^2 = 0.1$. It is quite apparent that the agreement between theory and both MD and DSMC simulations is excellent, with deviations appearing when the size ratio is large. As before, although not shown here, the agreement deteriorates with large contrast ($\lambda \geq 4$) and high density where, as mentioned, the approximations made by the theory become to be less valid.

Finally, in case III we study in more detail the density effects, which is done only using MD simulations as the DSMC method is not appropriate for this purpose. Specifically, Fig. 7 presents the normalized diffusion coefficient $D_0^*(\alpha)/D_0^*(1)$ as a function of the bath density $n\sigma^2$ for fixed coefficient of restitution and energy injection, and considering that particles are mechanically equivalent. In this situation, the theory predicts that there should be no density dependency on the scaled coefficient $D_0^*(\alpha)/D_0^*(1)$, while the MD results show that when increasing density there is an effect that can be as large as 20%. Note that the case under consideration in the figure is rather extreme, with low restitution coefficients (very high inelasticity) and large value of the contrast in Δ . Moderate cases do not present such strong deviation with density (not shown). These results are consistent with the hypothesis that the anomalous behavior of the MSD is due to correlations not included in the Enskog kinetic theory. These correlations play a relevant role on tracer diffusion at high densities and when the contrast between the tracer and the granular gas particles is large.

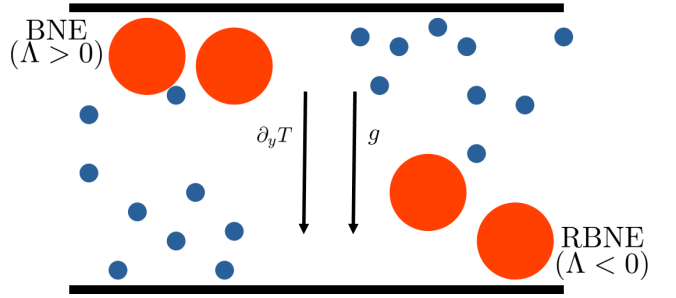


FIG. 8. Illustration of the segregation process behavior: small circles represent granular particles, and large circles represent impurities. The BNE ($\Lambda > 0$) effect occurs when the impurity rises to the top, while the RBNE ($\Lambda < 0$) effect occurs when the impurity sinks to the bottom of the system.

VII. THERMAL DIFFUSION SEGREGATION

One of the most usual phenomenon appearing in multi-component systems is the thermal diffusion segregation. It occurs in a non-convective steady state ($\mathbf{U} = \mathbf{0}$) due to the existence of a temperature gradient, which causes the movement of the different species of the mixture. In this situation, there is a balance between remixing of species caused by diffusion and segregation caused by temperature differences. The degree of segregation along the temperature gradient can be quantified by means of the so-called thermal diffusion factor Λ . In a steady state without convection ($\mathbf{U} = \mathbf{0}$) and where the mass flux is zero ($\mathbf{j}_0 = \mathbf{0}$), the thermal diffusion factor is defined as

$$-\Lambda \frac{\partial \ln T}{\partial y} = \frac{\partial}{\partial y} \ln \left(\frac{n_0}{n} \right). \quad (77)$$

Equation (77) has been simplified by assuming for the sake of simplicity that in the case of a two-dimensional system gradients occur only along the axis y . In addition, we also assume that the gravitational field is parallel to the thermal gradient, namely, $\mathbf{g} = -g\hat{e}_y$, where \hat{e}_y is the unit vector in the positive direction of the y axis.

Let us consider a scenario in which the tracer particles have a larger size than the granular gas particles ($\sigma_0 > \sigma$). Furthermore, as said before, since gravity and the thermal gradient align, then the lower plate is hotter than the upper plate ($\partial_y \ln T < 0$). Based on Eq. (77), when $\Lambda > 0$, impurities (or intruders) rise relative to granular gas particles ($\partial_z \ln(n_0/n) > 0$), leading to an accumulation of tracer particles near the cooler plate, known as the Brazil nut effect (BNE). Conversely, for $\Lambda < 0$, impurities descend compared to granular gas particles ($\partial_z \ln(n_0/n) < 0$), resulting in an accumulation near the hotter plate, giving rise to the Reverse Brazil Nut Effect (RBNE). An illustrative example of the segregation process for a two-dimensional system is shown in Fig. 8.

Let us determine the thermal diffusion factor. In the steady state, assuming that $\mathbf{j}_{0,y}^{(1)} = \mathbf{0}$ and $\mathbf{U} = \mathbf{0}$, the

momentum balance equation (13) reduces to $\partial_y p = -\rho g$. In dimensionless form, this relationship can be expressed as

$$p^* + \left(p^* + \phi \frac{\partial p^*}{\partial \phi} \right) \frac{\partial_y \ln n}{\partial_y \ln T} = -g^*, \quad (78)$$

where $g^* = \rho g / n \partial_y T < 0$ is a dimensionless parameter measuring the gravity relative to the thermal gradient. When we incorporate the condition $j_{0,y}^{(1)} = 0$ into Eq. (78), we can express the factor Λ in terms of the dimensionless diffusion coefficients D_0^* , D^* , and D_T^* :

$$\Lambda = \frac{\xi D_T^* - (D_0^* + D^*) (g^* + p^*)}{\xi D_0^*}, \quad (79)$$

where $\xi = p^* + \phi \partial_\phi p^*$. It is quite apparent from Eq. (79) that the effect on the different parameters of the system (impurity plus granular gas) on the signature of Λ is not simple at all. On the other hand, since Eq. (72) clearly shows that $D_0^* > 0$, then the curves delineating the regimes between the segregation toward the cold and the hot wall (BNE/RBNE transition) are determined from the condition

$$\xi D_T^* = (D_0^* + D^*) (g^* + p^*). \quad (80)$$

To disentangle the different competing mechanisms appearing in the constraint (80) it is convenient to consider first some limiting situations where a more simple criterion can be derived.

A. Mechanically equivalent particles

In this limiting case, $D_T^* = 0$, $D^* = -D_0^*$ and hence, Eq. (80) applies for any value of the coefficients of restitution, masses, diameters, solid volume fraction, and Δ parameters. In this case, as expected, no segregation appears in the system.

B. Low-density regime

Let us assume now a *dilute* granular gas ($n\sigma^2 \rightarrow 0$) in the absence of gravity ($|g^*| = 0$). In this limiting case, $p^* = \xi = 1$ and the (dimensionless) diffusion transport coefficients can be easily identified from Eqs. (66)–(68). According to these expressions, Eq. (80) yields the criterion

$$\tilde{\Delta}^* \frac{\partial \gamma_0}{\partial \tilde{\Delta}^*} \nu_D^* + (\gamma_0 - \mu) \Delta^* \frac{\partial \zeta^*}{\partial \Delta^*} = 0. \quad (81)$$

Equation (81) is still a quite complex relation in comparison with the one derived in the absence of gravity in the IHS model.³⁰ In this latter case, the segregation criterion is simply given by $\gamma_0 = \mu$.

When the inhomogeneities in both the density and temperature can be neglected ($\partial_z T \rightarrow 0$) but gravity is nonzero, then $|g^*| \rightarrow \infty$ (thermalized systems).

This situation (gravity dominates over thermal gradient) where segregation is essentially driven by gravity has been widely studied in simulations and experiments.^{53–56} In this limiting case, the segregation criterion in the low-density limit reads

$$\gamma_0 = \mu. \quad (82)$$

Equation (82) agrees with the results obtained in the IHS when the granular gas is heated by means of a stochastic thermostat.⁴⁷

C. Moderately dense regime

1. Absence of gravity ($|g^*| \rightarrow 0$)

Let us first consider a situation where gravity effects can be neglected ($|g^*| \rightarrow 0$). In this case, the condition $\Lambda = 0$ yields the relation

$$\xi D_T^* = (D_0^* + D^*) p^*. \quad (83)$$

Let us analyze the criterion established in Eq. (83) from a phenomenological perspective. In the complete absence of gravity and for dilute systems ($n\sigma^2 = 0$), the main factors influencing the segregation criterion are the thermal gradient and the energy loss or gain due to both collisions and the energy injected to the particles. Specifically, the BNE/RBNE transition will be determined by the balance of kinetic energy between the intruder and the granular gas. This balance is influenced by the energy loss from inelastic collisions (characterized by α and α_0) and by the external energy inputs (characterized by Δ and Δ_0).

Therefore, if the energy loss due to inelasticity and the energy input balance out for both species, no segregation will occur. However, if we modify the mechanical properties of each species, the number of collisions will vary. For instance, as established, we assume that the intruder is larger than the other granular particles, i.e., $\omega \equiv \sigma_0/\sigma > 1$. In this case, since the collision frequency ν_0 of the impurities is essentially proportional to σ_0 in a two-dimensional system, then the number of collisions experienced by them will increase. This leads to greater energy loss due to inelastic collisions. Nonetheless, it will also receive more energy from the external energy input parameter Δ_0 [see Eq. (6) when $\Delta = \Delta_0$], and the change in energy due to collisions will balance out.

To find a region where segregation occurs, we need to break the symmetry between impurities and the particles of the granular gas. For (dry) granular gases, this can be achieved by modifying the mechanical properties of the mixture. For example, larger particles experience more collisions, leading to greater energy loss. When the impurity is larger, it undergoes more collisions, ‘cools down’, and moves to the bottom wall (RBNE) since no extra velocity is added.^{31,34,57} In granular suspensions, the thermostat discriminates the interaction with species

based on their mechanical properties, thus promoting segregation.⁵⁰

In this work, we will break the symmetry by ensuring that the larger species (the impurity or intruder), which experiences more collisions, receives less energy input per collision. We will achieve this by setting a common coefficient of restitution ($\alpha = \alpha_0$) and imposing $\Delta_0 < \Delta$. Therefore, for a fixed mass ratio $\mu \equiv m_0/m$ and a sufficiently large diameter ratio ω , the intruder will lose energy and migrate to the bottom wall (RBNE). This effect can be observed in Fig. 9, where we illustrate a dilute two-dimensional system ($n\sigma^2 = 0$) with a common coefficient of restitution coefficient $\alpha = 0.9$, and $\Delta_0 = \Delta/2$. On the other hand, if we now fix ω and modify μ , we also observe a transition from BNE to RBNE as the intruder's mass increases. This result contrasts with those found in Ref. 58 for dilute granular mixtures, although it is important to note that the cited study considered arbitrary molar fractions.

As we decrease the contrast of energy parameter λ ($\Delta_0 = \lambda\Delta$), we intensify the symmetry breaking, apparently reinforcing the segregation criterion. However, the intruder loses so much energy that it is unable to penetrate the sea of granular particles near the upper (cold) plate, which move much faster, and eventually settles predominantly on the lower (hot) plate, resulting exclusively in RBNE (no segregation criterion can be found).

Let us now analyze the effect of density [or equivalently, the solid volume fraction $\phi = (\pi/4)n\sigma^2$] on segregation. As density increases, the frequency of collisions rises accordingly. For instance, if we maintain the same parameters as depicted in Fig. 9 but increase the density (e.g., by setting $\phi = 0.1$), locating a region where Λ cancels becomes more challenging. This phenomenon mirrors the difficulty observed in the dilute case when λ is too small. Consequently, to observe an expansion in the region where the BNE/RBNE transition occurs, we must mitigate the impact of collisions and energy loss in the intruder. This is achieved here by reducing α , but keeping $\alpha_0 = 0.9$. This expansion is evident in Fig. 10, where we have plotted two values of α : 0.6 and 0.9. However, the effect of density now causes that the disparity in particle density between cold and hot walls become increasingly apparent. This can lead to the intruder experiencing more collisions in the cold region, counteracting the effect of increased collisions due to higher kinetic energy in the hot zone. As a result, this interplay may lead to the inversion of the RBNE and BNE regions, as showed in Fig. 10. This marginal segregation curve qualitatively agrees with those obtained for moderately dense granular and molecular gases, with and without interstitial fluid,^{31,50} allowing for similar conclusions about the effect of density on segregation.

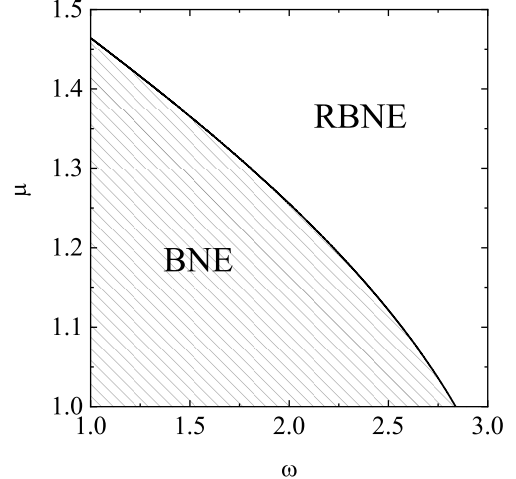


FIG. 9. Plot of the marginal segregation curve ($\Lambda = 0$) for a two-dimensional dilute ($n\sigma^2 \rightarrow 0$) system with a (common) coefficient of restitution $\alpha = \alpha_0 = 0.9$, and $|g^*| \rightarrow 0$. The points below the curve correspond to $\Lambda > 0$ (BNE), while the points above the curve correspond to $\Lambda < 0$ (RBNE). Here, $\Delta_0 = \Delta/2$.

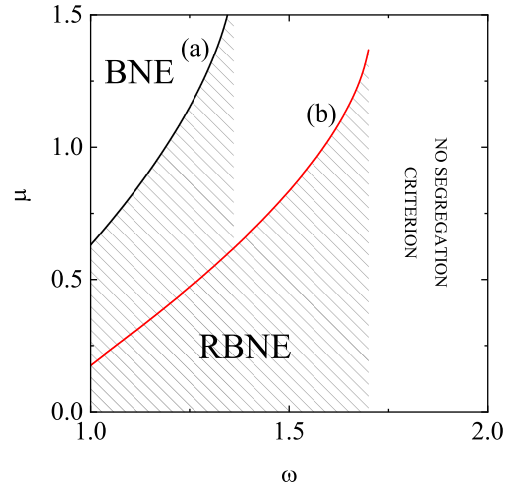


FIG. 10. Plot of the marginal segregation curve ($\Lambda = 0$) for $d = 2$, $\alpha_0 = 0.9$, $|g^*| \rightarrow 0$, $\phi = 0.1$, and two values of α : 0.9 (a) and 0.6 (b). The points below the curve correspond to $\Lambda < 0$ (RBNE), while the points above the curve correspond to $\Lambda > 0$ (BNE). Here, $\Delta_0 = \Delta/2$.

2. Thermalized systems ($\partial_z T \rightarrow 0$)

We will now examine a scenario where the segregation dynamics are primarily influenced by the gravitational force. In such cases, $|g^*| \rightarrow \infty$, making the temperature gradient negligible ($\partial_y T \rightarrow 0$) and the condition $\Lambda = 0$ yields the relation

$$D_0^* + D^* = 0. \quad (84)$$

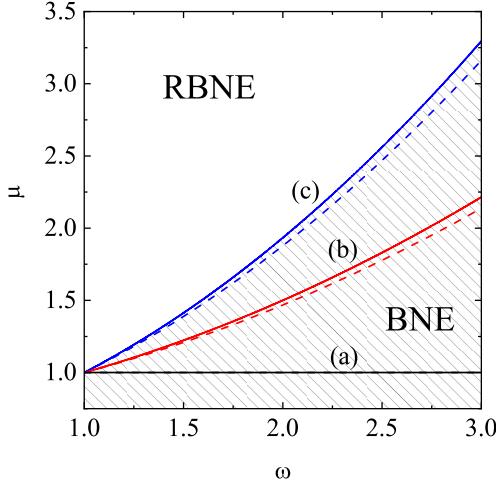


FIG. 11. Plot of the marginal segregation curve ($\Lambda = 0$) for $d = 2$, $\alpha = \alpha_0 = 0.8$ (solid lines) and 1 (dashed lines), $|g^*| \rightarrow \infty$, and three different values of the solid volume fraction ϕ : $\phi = 0$ (a), $\phi = 0.1$ (b), and $\phi = 0.2$ (c). The points below the curve correspond to $\Lambda > 0$ (BNE), while the points above the curve correspond to $\Lambda < 0$ (RBNE). Here, $\Delta = \Delta_0$.

Obtaining thermalized systems is achievable in experimental setups and numerical simulations that involve shaken or sheared systems.^{53,55,56,59} Figure 11 illustrates the segregation criterion for both a granular gas ($\alpha = \alpha_0 = 0.8$) and a molecular one ($\alpha = \alpha_0 = 1$). In this latter case, $\Delta = \Delta_0 = 0$ so that, we recover the segregation results for undriven granular mixtures.⁴⁹ Three different values of the volume fraction ϕ are considered in Fig. 11: $\phi = 0$, $\phi = 0.1$, and $\phi = 0.2$. Similar to driven granular mixtures (see Figs. 4 and 6 of Ref. 60 and Figs. 13 and 14 of Ref. 50), we observe a complete reversal of the RBNE/BNE transition when gravity is introduced, contrasting the phase diagrams shown in Fig. 10 for finite densities. Furthermore, both the effects of inelasticity and the injection of energy introduced by Δ and Δ_0 are suppressed by gravity, mimicking the behavior observed in granular suspensions and driven granular gases.^{50,60}

To provide an explanation for the BNE/RBNE transition, we can consider the interplay between particle mass and collision frequency. When intruder particles are heavier, their mass makes it easier for them to settle to the bottom of the container due to the effect of gravity, favoring the RBNE effect. Conversely, when the size ratio ω increases, tracer particles experience a higher number of collisions. These collisions induce a “buoyancy-like” effect on the intruder, driven by the pressure exerted by surrounding granular particles. Consequently, the intruder is effectively lifted against gravity, leading to the observation of the BNE effect. On the other hand, the effect of density, characterized by the volume fraction ϕ , is to increase the buoyancy effect, thus expanding the BNE region.

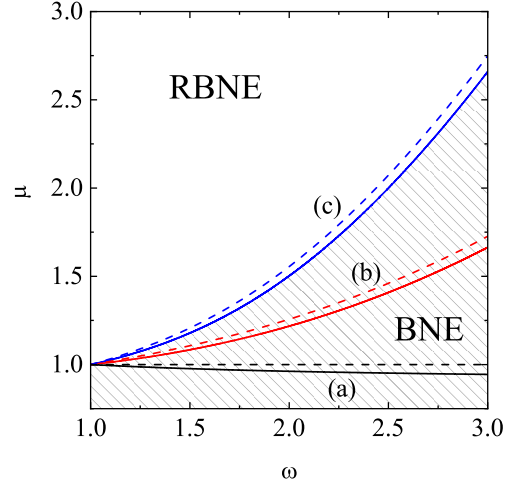


FIG. 12. Plot of the marginal segregation curve ($\Lambda = 0$) for $d = 2$, $\alpha = \alpha_0 = 0.8$ (solid lines) and 1 (dashed lines), $|g^*| = 1$, and three different values of the solid volume fraction ϕ : $\phi = 0$ (a), $\phi = 0.1$ (b), and $\phi = 0.2$ (c). The points below the curve correspond to $\Lambda > 0$ (BNE), while the points above the curve correspond to $\Lambda < 0$ (RBNE). Here, $\Delta = \Delta_0$.

3. General case

Finally, we examine the general case where the impact of the temperature gradient is comparable to that of gravity. To exemplify this, Fig. 12 displays the marginal segregation curve for a reduced gravity $|g^*| = 1$ and for the same systems as plotted in Fig. 11.

The primary conclusion to be drawn is that, similar to dry granular mixtures and granular suspensions,^{34,50} the effect of gravity is significantly more pronounced than that of the thermal gradient, as the BNE/RBNE transition is maintained. Additionally, the influence of inelasticity is also notably attenuated. Furthermore, in alignment with thermalized cases, an increase in density enlarges the region where the BNE effect is observed. Since ordinary temperature plays no role in the motion of grains, at the core of statistical description we can establish an equivalence between the density and the external driving in terms of the kinetic energy provided to the particles. Therefore, an analogy can be drawn between adjusting density and altering the shaking strength in experimental setups.^{61,62} Specifically, decreasing the shaking strength expands the BNE region. This phenomenon has already been observed in freely evolving and driven granular mixtures, as well as in granular suspensions.^{34,50}

VIII. DISCUSSION

In this work, we have considered a kinetic theory approach to determine the diffusion transport coefficients for a granular binary mixture in the tracer limit. The injection of energy in the system is accounted for by a col-

lisional model, the so-called Δ -model.⁸ In particular, in each collision an amount of relative velocity Δ is added to the velocities of the colliding particles. This energy injection acts as an effective thermostat, allowing the system to reach a steady state.^{9,10}

It should be noted that in a granular binary mixture (composed of two types of particles differing in mass, diameter, inelasticity, or the value of Δ at collisions), the steady state of the Δ -model is characterized by a temperature ratio T_1/T_2 different from 1 (breakdown of the energy equipartition). Although the granular temperature T is the relevant one at a hydrodynamic level, the effect of the energy nonequipartition on transport must be accounted for since its impact on transport is generally significant, as has been clearly shown in previous works for IHS [see for instance, the review 63].

In the tracer limit, since the state of the granular gas (excess component) is not affected by the presence of tracer or impurity particles, the momentum and heat fluxes of the system (impurities plus granular gas) are the same as that for the granular gas. In this limiting case the mass flux of the impurities \mathbf{j}_0 is the relevant flux of the problem, and therefore the goal of this paper has been to determine \mathbf{j}_0 in terms of the parameter space of the system.

The theoretical framework of our study is based on the Enskog kinetic equation, which extends the Boltzmann results for low-density gases to higher densities. Under the tracer condition, the kinetic equation for the velocity distribution function f of the granular gas decouples from the tracer velocity distribution function f_0 , and thus the distribution f obeys the usual nonlinear Enskog equation. In addition, since the collisions between the tracer particles themselves can be neglected, the distribution f_0 obeys a linear Enskog–Lorentz kinetic equation.

In the Navier–Stokes domain, the constitutive equation for the mass flux $\mathbf{j}_0^{(1)}$ is given by Eq. (1), where the superscript 1 in \mathbf{j}_0 means that the flux is computed to first order in the spatial gradients of n_0 , n , and T . Equation (1) includes three transport coefficients: (a) the tracer diffusion coefficient, D_0 , associated with the gradient of tracer concentration ∇n_0 , (b) the mutual diffusion coefficient, D , related with the diffusion of impurities into the bulk particles; it is associated with the density gradient ∇n , and (c) the thermal diffusion coefficient, D_T , associated with the temperature gradient ∇T . These three coefficients have been obtained here in the so-called first Sonine approximation, with results expressed in Eqs. (53)–(55). While the first Sonine approximation simplifies the solution of the coupled integral equations, higher order terms in the Sonine expansion may be necessary to achieve greater accuracy, especially in extreme conditions such as very strong inelasticity and/or very disparate mass and diameter ratios.

To assess the validity of the analytical predictions, numerical simulations were performed for the tracer diffusion coefficient, D_0 . Its value is obtained by differentiating, with respect to time, the mean square displacement

of the tracer particles at long times, when the diffusive limit is reached. Two simulation techniques have been employed: the DSMC method^{28,51} and MD simulations using the event-driven method.^{25–27} The DSMC method provides “exact” solutions of the kinetic equation beyond the first Sonine polynomial approximation. Thus, deviations of DSMC simulations from the (approximate) analytical results could in principle be mitigated by considering higher-order Sonine corrections to the distribution functions f and f_0 . MD simulations, however, do not rely on the assumptions of the Enskog kinetic equation, such as the molecular chaos assumption, the form of the pair correlation function or any other correlations ignored in the theoretical description.

It is interesting to note that the MD simulations show an intermediate regime between the short-time (ballistic) and the long-time (diffusive) regimes (see Fig. 4); it deserves further study. This new regime is particularly noticeable when the dynamic properties of the impurity are very different from those of the bulk (granular gas particles); in particular, when the energy input to the tracer particles is greater than that to the particles of the granular gas.

The results show that the agreement between the analytical and numerical results is excellent for moderate densities and not very strong inelasticities, as expected. However, as the dissipation and density increase, some discrepancies between simulations and theoretical results appear. The discrepancy between theory and DSMC simulations is rather small and has its origin in the first Sonine approximation considered in the theoretical development. MD simulations, however, show larger deviations from the theoretical results, which may be related to the breakdown of the molecular chaos hypothesis, especially at high densities.

As an application of the derived expressions for the diffusion transport coefficients, the thermal diffusion factor Λ [defined in Eq. (77)] was obtained. The evaluation of Λ provides new insights into the segregation phenomenon in dense granular mixtures in the presence of gravity and/or a temperature gradient. The phase diagrams obtained for the transition between the BNE and the RBNE^{64,65} provide a more comprehensive understanding of how variations in system parameters such as mass, size and inelasticity control segregation. The results suggest that segregation dynamics in confined granular systems differ significantly from those in driven or freely cooling systems of IHS,^{30,31,48,60} reiterating the fact that energy input can influence segregation criteria. On the other hand, a similar behavior has been observed in some situations with the phase diagrams of segregation obtained for granular suspensions.⁵⁰

Despite the success of the current theoretical framework, future work could focus on refining the analytical expressions for the diffusion coefficients, perhaps by using alternative methods for solving the Enskog–Lorentz equation or by exploring higher order terms in the Sonine polynomial expansion. In addition, the interplay between

confinement, inelasticity, and particle shape could be further investigated, as these factors are likely to influence transport properties in granular gases under more complex conditions.

In summary, the present study provides a comprehensive theoretical treatment of mass transport in a dense granular gas within a confined geometry, providing valuable predictions for tracer diffusion coefficients. The results highlight the usefulness of the Δ model in mimicking energy transfer between the horizontal and vertical degrees of freedom, and the comparison with simulation data confirms the validity of the theoretical approach. The work also extends previous findings by introducing a segregation criterion that distinguishes between BNE and RBNE under a thermal gradient and gravity, contributing to a broader understanding of granular segregation in confined systems.

ACKNOWLEDGMENTS

The work of R.G.G. and V.G. is supported from Grant No. PID2020-112936GB-I00 funded by MCIN/AEI/10.13039/501100011033. The work of R.B. is supported from Grant Number PID2020-113455GB-I00 and PID2023-147067NB-I00. The work of R.S. is supported by the Fondecyt Grant No. 1220536 and Millennium Science Initiative Program NCN19_170 of ANID, Chile.

AUTHOR DECLARATIONS

In this Appendix we provide some technical details on the evaluation of the diffusion transport coefficients by considering the first Sonine approximations (50)–(52). Let us evaluate each transport coefficient separately.

1. Tracer diffusion coefficient D_0

We consider first the tracer diffusion coefficient D_0 . In this case, \mathbf{B}_0 is given by Eq. (51) and Eq. (42) yields

$$d\frac{m_0\rho_0}{\rho}\zeta^{(0)}T\partial_TD_0 + \frac{m_0^2}{\rho T_0}D_0 \int d\mathbf{v} m_0\mathbf{V}\cdot\mathbf{J}_0^{(0)}\left[f_{0M}\mathbf{V}, f^{(0)}\right] = -dn_0T_0^{(0)}, \quad (\text{A1})$$

where $\rho_0 = m_0n_0$ and use has been made of the result

$$\int d\mathbf{v} m_0\mathbf{V}\cdot\mathbf{B}_0 = -dn_0T_0^{(0)}. \quad (\text{A2})$$

Equation (A1) can be rewritten in terms of the dimensionless coefficient $D_0^* = (m_0^2\nu/\rho T)D_0$ as

$$-\frac{1}{2}\zeta^*D_0^*\left(1 - \tilde{\Delta}^*\frac{\partial \ln D_0^*}{\partial \tilde{\Delta}^*}\right) + \nu_D^*D_0^* = \gamma_0, \quad (\text{A3})$$

where we recall that $\zeta^* = \zeta^{(0)}/\nu$, $\gamma_0 = T_0^{(0)}/T$ and

$$\nu_D^* = -\frac{1}{dn_0T_0^{(0)}\nu} \int d\mathbf{v} m_0\mathbf{V}\cdot\mathbf{J}_0^{(0)}\left[f_{0M}\mathbf{V}, f^{(0)}\right]. \quad (\text{A4})$$

Upon obtaining Eq. (A3), we have taken into account that

$$T\partial_TD_0^* = -\frac{1}{2}\tilde{\Delta}^*\frac{\partial D_0^*}{\partial \tilde{\Delta}^*}. \quad (\text{A5})$$

Conflict of Interest

The authors have no conflicts to disclose.

Author Contributions

Rubén Gómez González: Formal analysis (equal); Investigation (equal); Writing–review&editing (equal).

Vicente Garzo: Formal analysis (equal); Investigation (equal); Writing/Original Draft Preparation (lead); Writing–review&editing(equal).

Ricardo Brito: Conceptualization (equal); Investigation (equal); Software (lead); Writing–review&editing(equal).

Rodrigo Soto: Conceptualization(equal); Investigation (equal); Software (lead); Writing–review&editing (equal).

DATA AVAILABILITY

The data that support the findings of this study are available from the corresponding author upon reasonable request.

Appendix A: First Sonine approximation to the diffusion transport coefficients

The expression of ν_D^* was estimated in Ref. 21 when the zeroth-order distribution $f^{(0)}(\mathbf{V})$ of the granular gas is approximated by the Maxwellian distribution (18) with the replacement $\mathbf{v} \rightarrow \mathbf{V}$. In this approximation, one gets the result

$$\nu_D^* = \frac{2\pi^{\frac{d-1}{2}}}{d\Gamma\left(\frac{d}{2}\right)} \chi_0 \left(\frac{\bar{\sigma}}{\sigma}\right)^{d-1} M \left[\left(\frac{1+\theta}{\theta}\right)^{1/2} (1+\alpha_0) + \sqrt{\pi} \Delta_0^* \right]. \quad (\text{A6})$$

In the HSS, $\zeta^* = 0$ and Eq. (A3) gives the expression (53) for D_0^* .

2. Thermal diffusion coefficient D_T

In a similar way as D_0 , the thermal diffusion coefficient D_T can be easily obtained from Eqs. (41) and (50) as

$$d\rho\zeta^{(0)}T\partial_T D_T + \frac{1}{2}d\rho\zeta^{(0)}\left(1 - \Delta^* \frac{\partial \ln \zeta^*}{\partial \Delta^*}\right)D_T - d\rho\nu\nu_D^* D_T = \int d\mathbf{v} m_0 \mathbf{V} \cdot \mathbf{A}_0. \quad (\text{A7})$$

According to the expression (44) of \mathbf{A}_0 , the right hand side of Eq. (A7) can be computed as

$$\int d\mathbf{v} m_0 \mathbf{V} \cdot \mathbf{A}_0 = -dn_0 T \left(\gamma_0 - \frac{1}{2} \tilde{\Delta}^* \frac{\partial \gamma_0}{\partial \tilde{\Delta}^*} \right) + d\frac{\rho_0}{\rho} p \left(1 - \frac{1}{2} \Delta^* \frac{\partial \ln p^*}{\partial \Delta^*} \right) - \int d\mathbf{v} m_0 \mathbf{V} \cdot \mathcal{K}_0 \left[T \frac{\partial f^{(0)}}{\partial T} \right], \quad (\text{A8})$$

where

$$\Delta^* \frac{\partial p^*}{\partial \Delta^*} = \frac{2^d}{\sqrt{2\pi}} \chi \phi \Delta^*. \quad (\text{A9})$$

Equation (A7) can be rewritten in terms of the dimensionless coefficient $D_T^* = (\rho\nu/n_0 T)D_T$ as

$$\begin{aligned} \frac{1}{2} \zeta^* D_T^* \left(1 - \tilde{\Delta}^* \frac{\partial \ln D_T^*}{\partial \tilde{\Delta}^*} \right) + \frac{1}{2} \zeta^* D_T^* \left(1 - \Delta^* \frac{\partial \ln \zeta^*}{\partial \Delta^*} \right) - \nu_D^* D_T^* &= -\gamma_0 \left(1 - \frac{1}{2} \tilde{\Delta}^* \frac{\partial \ln \gamma_0}{\partial \tilde{\Delta}^*} \right) + \frac{m_0}{m} \left(p^* - \frac{2^{d-1}}{\sqrt{2\pi}} \chi \phi \Delta^* \right) \\ &- \frac{1}{dn_0 T} \int d\mathbf{v} m_0 \mathbf{V} \cdot \mathcal{K}_0 \left[T \frac{\partial f^{(0)}}{\partial T} \right]. \end{aligned} \quad (\text{A10})$$

The collision integral involving the operator \mathcal{K}_0 has been evaluated in the Appendix B with the result

$$\frac{1}{dn_0 T} \int d\mathbf{v} m_0 \mathbf{V} \cdot \mathcal{K}_0 \left[T \frac{\partial f^{(0)}}{\partial T} \right] = 2^d \left(\frac{\bar{\sigma}}{\sigma} \right)^d \phi \chi_0 M_0 \left[\frac{1+\alpha_0}{2} + \frac{\Delta_0^*}{\sqrt{\pi}} \left(\frac{\theta}{1+\theta} \right)^{1/2} \right]. \quad (\text{A11})$$

In the HSS ($\zeta^* = 0$), the differential equation (A10) becomes an algebraic equation whose solution gives Eq. (54) for D_T^* .

3. Diffusion coefficient \mathbf{D}

In the case of the diffusion coefficient D , \mathbf{C}_0 is given by Eq. (52). As for D^* and D_T^* , the equation for the dimensionless diffusion coefficient D_0^* can be derived from Eq. (57) (with $\mathbf{C} = \mathbf{0}$) by multiplying both sides of this equation by $m_0 \mathbf{V}$ and integrating on velocity. The result is

$$\frac{1}{2} \zeta^* D^* \left(1 - \tilde{\Delta}^* \frac{\partial \ln D^*}{\partial \tilde{\Delta}^*} \right) - \nu_D^* D^* = \frac{1}{dn_0 T} \int d\mathbf{v} m_0 \mathbf{V} \cdot \mathbf{C}_0 - \zeta^* \left(1 + \phi \frac{\partial \ln \chi}{\partial \phi} \right) D_T^*, \quad (\text{A12})$$

where $D^* = (m_0 \nu / n_0 T)D$. The first term on the right-hand side of Eq. (A12) is given by

$$\frac{1}{dn_0 T} \int d\mathbf{v} m_0 \mathbf{V} \cdot \mathbf{C}_0 = -\phi \frac{\gamma_0}{\partial \phi} + \mu \left(p^* + \phi \frac{\partial p^*}{\partial \phi} \right) - \frac{(1+\omega)^{-d}}{\chi_0 T} \left(\frac{\partial \mu_0}{\partial \phi} \right)_{T,n_0} \frac{1}{dn_0 T} \int d\mathbf{v} m_0 \mathbf{V} \cdot \mathcal{K}_0 \left[f^{(0)} \right]. \quad (\text{A13})$$

In Eq. (A13), we recall that $\mu = m_0/m$ and $\omega = \sigma_0/\sigma$. The collisional integral appearing in the last term on the right hand side of Eq. (A13) has been also computed in the Appendix B with the result

$$\frac{1}{dn_0 T} \int d\mathbf{v} m_0 \mathbf{V} \cdot \mathcal{K}_0 \left[f^{(0)} \right] = 2^d \left(\frac{\bar{\sigma}}{\sigma} \right)^d \phi \chi_0 M_0 \left(\frac{1+\theta}{\theta} \right) \left[\frac{1+\alpha_0}{2} + \frac{2\Delta_0^*}{\sqrt{\pi}} \left(\frac{\theta}{1+\theta} \right)^{1/2} \right]. \quad (\text{A14})$$

The expression (55) for D^* in the HSS can be easily obtained when one takes $\zeta^* = 0$ in Eq. (A12) and takes into account Eqs. (A13) and (A14).

4. Derivatives with respect to Δ^* and $\tilde{\Delta}^*$

It is readily apparent that the diffusion transport coefficients are given in terms of some derivatives. Let us evaluate these derivatives in the HSS. We start with the derivative $\partial\gamma_0/\partial\phi$ in the steady state ($\zeta^* = \zeta_0^* = 0$). It can be obtained from the time-dependent equation for the temperature ratio γ_0 :

$$\zeta^* \tilde{\Delta}^* \frac{\partial\gamma_0}{\partial\tilde{\Delta}^*} = 2\gamma_0 (\zeta^* - \zeta_0^*). \quad (\text{A15})$$

In the steady state, Eq. (A15) is trivially satisfied. To determine the derivative $\partial\gamma_0/\partial\phi$ at the steady state, we take first the derivative with respect to ϕ in both sides of Eq. (A15) and then takes the steady state limit. Thus, one gets the identity

$$\frac{\partial\tilde{\zeta}_0}{\partial\phi} = \frac{\partial\tilde{\zeta}_0}{\partial\gamma_0} \frac{\partial\gamma_0}{\partial\phi} = 0, \quad (\text{A16})$$

where $\tilde{\zeta}_0 = \zeta_0^*/\chi_0$. Upon obtaining Eq. (A16) use has been made of the fact that in the steady state $\partial\zeta^*/\partial\phi = \zeta^*(\partial\ln\chi/\partial\phi) = 0$ and $\tilde{\zeta}_0 = 0$. Since in Eq. (A16), $\partial\tilde{\zeta}_0/\partial\gamma_0$ is in general different from zero in the steady state, then one concludes that $\partial\gamma_0/\partial\phi = 0$ in the steady state for the Δ -model.

In addition, the derivative $\partial\gamma_0/\partial\tilde{\Delta}$ can be also be obtained from Eq. (A15). It is given by

$$\tilde{\Delta}^* \frac{\partial\gamma_0}{\partial\tilde{\Delta}^*} = \gamma_0 \frac{\Delta^* \frac{\partial\zeta^*}{\partial\Delta^*} - \tilde{\Delta}^* \left(\frac{\partial\zeta_0^*}{\partial\Delta^*} \right)_{\gamma_0}}{\frac{1}{2} \Delta^* \frac{\partial\zeta^*}{\partial\Delta^*} + \gamma_0 \left(\frac{\partial\zeta_0^*}{\partial\gamma_0} \right)_{\tilde{\Delta}^*}}, \quad (\text{A17})$$

where

$$\Delta^* \frac{\partial\zeta^*}{\partial\Delta^*} = -\frac{\sqrt{2}\pi^{\frac{d-1}{2}}}{d\Gamma\left(\frac{d}{2}\right)} \chi(\phi) \Delta^* \left(4\Delta^* + \sqrt{2\pi}\alpha \right), \quad \tilde{\Delta}^* \frac{\partial\zeta_0^*}{\partial\tilde{\Delta}^*} = \Delta_0^* \frac{\partial\zeta_0^*}{\partial\Delta_0^*}. \quad (\text{A18})$$

Appendix B: Evaluation of the collision integrals

In this Appendix we compute the collision integrals appearing in the evaluation of the transport coefficients D_T and D . Let us start with the collision integral

$$I_{D_T} \equiv \int d\mathbf{v} m_0 \mathbf{V} \cdot \mathcal{K}_0 \left[T \frac{\partial f^{(0)}}{\partial T} \right] \quad (\text{B1})$$

This integral can be computed by using the property

$$\int d\mathbf{v}_1 \psi(\mathbf{V}_1) \mathcal{K}_{0,i} [X(\mathbf{V}_2)] = -\bar{\sigma}^d \chi_0 \int d\mathbf{V}_1 \int d\mathbf{V}_2 \int d\hat{\sigma} \Theta(\hat{\sigma} \cdot \mathbf{g}_{12}) (\hat{\sigma} \cdot \mathbf{g}_{12}) \hat{\sigma}_i f_0^{(0)}(\mathbf{V}_1) X(\mathbf{V}_2) [\psi(\mathbf{V}'_1) - \psi(\mathbf{V}_1)], \quad (\text{B2})$$

where we recall that \mathbf{V}'_1 is defined by

$$\mathbf{V}'_1 = \mathbf{V}_1 - M(1 + \alpha_0) (\hat{\sigma} \cdot \mathbf{g}_{12}) \hat{\sigma} - 2M\Delta_0 \hat{\sigma}. \quad (\text{B3})$$

Using the property (B2), the integral I_{D_T} reads

$$\begin{aligned} I_{D_T} &= -m_0 \bar{\sigma}^d \chi_0 \int d\mathbf{V}_1 \int d\mathbf{V}_2 \int d\hat{\sigma} \Theta(\hat{\sigma} \cdot \mathbf{g}_{12}) (\hat{\sigma} \cdot \mathbf{g}_{12}) f_0^{(0)}(\mathbf{V}_1) \left[T \frac{\partial f^{(0)}(\mathbf{V}_2)}{\partial T} \right] \hat{\sigma} \cdot (\mathbf{V}'_1 - \mathbf{V}_1) \\ &= m_0 M \bar{\sigma}^d \chi_0 \int d\mathbf{V}_1 \int d\mathbf{V}_2 \int d\hat{\sigma} \Theta(\hat{\sigma} \cdot \mathbf{g}_{12}) (\hat{\sigma} \cdot \mathbf{g}_{12}) f_0^{(0)}(\mathbf{V}_1) \left[T \frac{\partial f^{(0)}(\mathbf{V}_2)}{\partial T} \right] \left[(1 + \alpha_0) (\hat{\sigma} \cdot \mathbf{g}_{12}) + 2\Delta_0 \right]. \end{aligned} \quad (\text{B4})$$

In the hydrodynamic regime, the zeroth-order distribution function $f^{(0)}(\mathbf{V})$ of the granular gas has the scaled form

$$f^{(0)}(\mathbf{V}) = n v_0^{-d} \varphi(\mathbf{c}, \Delta^*), \quad (\text{B5})$$

where $\mathbf{c} = \mathbf{V}/v_0$ and the unknown scaled distribution φ depends on T through \mathbf{c} and Δ^* . According to Eq. (B5), $f^{(0)}(\mathbf{V})$ has the property

$$T \frac{\partial f^{(0)}}{\partial T} = -\frac{1}{2} \frac{\partial}{\partial \mathbf{V}} \cdot (\mathbf{V} f^{(0)}) - \frac{1}{2} n v_0^{-d} \Delta^* \frac{\partial \varphi}{\partial \Delta^*}. \quad (\text{B6})$$

However, if one takes the Maxwellian approximation (18) for $f^{(0)}(\mathbf{V})$, then $\varphi \simeq \pi^{-d/2} e^{-c^2}$, and so

$$T \frac{\partial f^{(0)}}{\partial T} \simeq -\frac{1}{2} \frac{\partial}{\partial \mathbf{V}} \cdot (\mathbf{V} f^{(0)}). \quad (\text{B7})$$

For the sake of simplicity, the approximation (B7) is employed here to evaluate I_{D_T} . In this case,

$$\begin{aligned} I_{D_T} &= -\frac{1}{2} m_0 M \bar{\sigma}^d \chi_0 \int d\mathbf{V}_1 \int d\mathbf{V}_2 f_0^{(0)}(\mathbf{V}_1) \frac{\partial}{\partial V_{2i}} \left(V_{2i} f^{(0)}(\mathbf{V}_2) \right) \int d\hat{\sigma} \Theta(\hat{\sigma} \cdot \mathbf{g}_{12}) (\hat{\sigma} \cdot \mathbf{g}_{12}) \left[(1 + \alpha_0) (\hat{\sigma} \cdot \mathbf{g}_{12}) + 2\Delta_0 \right] \\ &= -\frac{1}{2} m_0 M \bar{\sigma}^d \chi_0 \int d\mathbf{V}_1 \int d\mathbf{V}_2 f_0^{(0)}(\mathbf{V}_1) \frac{\partial}{\partial V_{2i}} \left(V_{2i} f^{(0)}(\mathbf{V}_2) \right) \left[B_2 (1 + \alpha_0) g_{12}^2 + 2B_1 \Delta_0 g_{12} \right], \end{aligned} \quad (\text{B8})$$

where

$$B_k = \pi^{(d-1)/2} \frac{\Gamma(\frac{k+1}{2})}{\Gamma(\frac{k+d}{2})}. \quad (\text{B9})$$

The integral I_{D_T} can be split in two parts; one of them was already computed³⁷ when $\Delta_0 = 0$. Thus, the integral I_{D_T} can be written as

$$I_{D_T} = I_{D_T}^{(0)} + I_{D_T}^{(1)}, \quad (\text{B10})$$

where³⁷

$$I_{D_T}^{(0)} = dB_2 n \bar{\sigma}^d \chi_0 M_0 n_0 T (1 + \alpha_0), \quad (\text{B11})$$

and

$$I_{D_T}^{(1)} = -B_1 m_0 M \bar{\sigma}^d \chi_0 \Delta_0 \int d\mathbf{V}_1 \int d\mathbf{V}_2 f_0^{(0)}(\mathbf{V}_1) \frac{\partial}{\partial V_{2i}} \left(V_{2i} f^{(0)}(\mathbf{V}_2) \right) g_{12}. \quad (\text{B12})$$

Integrating by parts, Eq. (B11) can be written as

$$\begin{aligned} I_{D_T}^{(1)} &= B_1 m_0 M \bar{\sigma}^d \chi_0 \Delta_0 \int d\mathbf{V}_1 \int d\mathbf{V}_2 f_0^{(0)}(\mathbf{V}_1) f^{(0)}(\mathbf{V}_2) V_{2i} \frac{\partial g_{12}}{\partial V_{2i}} \\ &= -B_1 m_0 M \bar{\sigma}^d \chi_0 \Delta_0 \int d\mathbf{V}_1 \int d\mathbf{V}_2 f_0^{(0)}(\mathbf{V}_1) f^{(0)}(\mathbf{V}_2) g_{12}^{-1} (\mathbf{g}_{12} \cdot \mathbf{V}_2). \end{aligned} \quad (\text{B13})$$

To evaluate the integral (B13), we approximate $f_0^{(0)}(\mathbf{V}_1)$ and $f^{(0)}(\mathbf{V}_2)$ by their Maxwellian forms:

$$f_0^{(0)}(\mathbf{V}_1) \rightarrow n_0 \left(\frac{m_0}{2\pi T_0^{(0)}} \right)^{d/2} \exp \left(-\frac{m_0 V_1^2}{2T_0^{(0)}} \right), \quad f^{(0)}(\mathbf{V}_2) \rightarrow n \left(\frac{m}{2\pi T} \right)^{d/2} \exp \left(-\frac{m V_2^2}{2T} \right). \quad (\text{B14})$$

Using these Maxwellian distributions, Eq. (B13) can be expressed as

$$I_{D_T}^{(1)} = -B_1 \pi^{-d} m_0 M n \bar{\sigma}^d n_0 \chi_0 \Delta_0^* v_0^2 \theta^{d/2} I_{D_T}^{(1)*}, \quad (\text{B15})$$

where the (dimensionless) integral $I_{D_T}^{(1)*}$ is

$$I_{D_T}^{(1)*} = \int d\mathbf{c}_1 \int d\mathbf{c}_2 g_{12}^{*-1} (\mathbf{g}_{12}^* \cdot \mathbf{c}_2) e^{-\theta c_1^2 - c_2^2}. \quad (\text{B16})$$

Here, $\mathbf{g}_{12}^* = \mathbf{g}_{12}/v_0$, $\mathbf{c}_1 = \mathbf{V}_1/v_0$, $\mathbf{c}_2 = \mathbf{V}_2/v_0$, and $\theta = m_0 T / m T_0^{(0)}$. The integral (B16) can be performed by the change of variables $\mathbf{x} = \mathbf{c}_1 - \mathbf{c}_2$ and $\mathbf{y} = \theta \mathbf{c}_1 + \mathbf{c}_2$, with the Jacobian $(1 + \theta)^{-d}$. The result is

$$I_{D_T}^{(1)*} = -\pi^d \frac{\Gamma\left(\frac{d+1}{2}\right)}{\Gamma\left(\frac{d}{2}\right)} \theta^{\frac{1-d}{2}} (1 + \theta)^{-1/2}. \quad (\text{B17})$$

With this result, the final expression of $I_{D_T}^{(1)}$ is

$$I_{D_T}^{(1)} = \frac{2^d d}{\sqrt{\pi}} M_0 \left(\frac{\bar{\sigma}}{\sigma}\right)^d \phi \chi_0 \left(\frac{\theta}{1 + \theta}\right)^{1/2} \Delta_0^* n_0 T, \quad (\text{B18})$$

where Eq. (17) has been employed. According to Eqs. (B11) and (B18), the expression of I_{D_T} can be finally written as

$$I_{D_T} = 2^d d \left(\frac{\bar{\sigma}}{\sigma}\right)^d \phi \chi_0 M_0 n_0 T \left[\frac{1 + \alpha_0}{2} + \frac{\Delta_0^*}{\sqrt{\pi}} \left(\frac{\theta}{1 + \theta}\right)^{1/2} \right]. \quad (\text{B19})$$

We consider now the collisional integral

$$I_D \equiv \int d\mathbf{v} m_0 \mathbf{V} \cdot \mathcal{K}_0 \left[f^{(0)} \right]. \quad (\text{B20})$$

By employing the property (B2), one easily gets

$$\begin{aligned} I_D &= m_0 M \bar{\sigma}^d \chi_0 \int d\mathbf{V}_1 \int d\mathbf{V}_2 \int d\hat{\sigma} \Theta(\hat{\sigma} \cdot \mathbf{g}_{12}) (\hat{\sigma} \cdot \mathbf{g}_{12}) f_0^{(0)}(\mathbf{V}_1) f^{(0)}(\mathbf{V}_2) \left[(1 + \alpha_0) (\hat{\sigma} \cdot \mathbf{g}_{12}) + 2\Delta_0 \right] \\ &= m_0 M \bar{\sigma}^d \chi_0 \int d\mathbf{V}_1 \int d\mathbf{V}_2 f_0^{(0)}(\mathbf{V}_1) f^{(0)}(\mathbf{V}_2) \left[B_2 g_{12}^2 (1 + \alpha_0) + 2B_1 g_{12} \Delta_0 \right]. \end{aligned} \quad (\text{B21})$$

As in the case of the integral I_{D_T} , I_D can be split in two parts; one of them has been already computed when $\Delta_0 = 0$. Thus,

$$I_D = I_D^{(0)} + I_D^{(1)}, \quad (\text{B22})$$

where³⁷

$$I_D^{(0)} = 2^{d-1} d \left(\frac{\bar{\sigma}}{\sigma}\right)^d \phi \chi_0 M_0 \left(\frac{1 + \theta}{\theta}\right) (1 + \alpha_0) n_0 T, \quad (\text{B23})$$

and

$$I_D^{(1)} = \frac{2\pi^{(d-1)/2}}{\Gamma\left(\frac{d+1}{2}\right)} m_0 M \bar{\sigma}^d \chi_0 \Delta_0 \int d\mathbf{V}_1 \int d\mathbf{V}_2 g_{12} f_0^{(0)}(\mathbf{V}_1) f^{(0)}(\mathbf{V}_2). \quad (\text{B24})$$

The integral $I_D^{(1)}$ can be also evaluated by replacing $f_0^{(0)}(\mathbf{V}_1)$ and $f^{(0)}(\mathbf{V}_2)$ by their Maxwellian approximations (B14). The result is

$$I_D^{(1)} = \frac{2^{d+1} d}{\sqrt{\pi}} \left(\frac{\bar{\sigma}}{\sigma}\right)^d \phi \chi_0 M_0 \Delta_0^* \left(\frac{1 + \theta}{\theta}\right)^{1/2} n_0 T. \quad (\text{B25})$$

With this result, the expression of I_D can be written as

$$I_D = 2^d d \left(\frac{\bar{\sigma}}{\sigma}\right)^d \phi \chi_0 M_0 \left(\frac{1 + \theta}{\theta}\right) n_0 T \left[\frac{1 + \alpha_0}{2} + \frac{2\Delta_0^*}{\sqrt{\pi}} \left(\frac{\theta}{1 + \theta}\right)^{1/2} \right]. \quad (\text{B26})$$

¹J. S. Olafsen and J. S. Urbach, “Clustering, order, and collapse

in a driven granular monolayer,” Phys. Rev. Lett. **81**, 4369–4372

(1998).

²A. Prevost, P. Melby, D. A. Egolf, and J. S. Urbach, "Nonequilibrium two-phase coexistence in a confined granular layer," *Phys. Rev. E* **70**, 050301 (2004).

³P. Melby, F. V. Reyes, A. Prevost, R. Robertson, P. Kumar, D. A. Egolf, and J. S. Urbach, "The dynamics of thin vibrated granular layers," *Journal of Physics: Condensed Matter* **17**, S2689 (2005).

⁴N. Mujica and R. Soto, "Dynamics of noncohesive confined granular media," in *Recent Advances in Fluid Dynamics with Environmental Applications* (Springer), 445–463 (2016).

⁵M. Mayo, J. J. Brey, M. I. García Soria, and P. Maynar, "Kinetic theory of a confined quasi-one-dimensional gas of hard disks," *Physica A* **597**, 127237 (2022).

⁶P. Maynar, M. I. García Soria, and J. J. Brey, "Dynamics of an inelastic tagged particle under strong confinement," *Phys. Fluids* **34**, 123321 (2022).

⁷M. Mayo, J. C. Petit, M. I. García Soria, and P. Maynar, "Confined granular gases under the influence of vibrating walls," *J. Stat. Mech.* **123208** (2023).

⁸R. Brito, D. Risso, and R. Soto, "Hydrodynamic modes in a confined granular fluid," *Phys. Rev. E* **87**, 022209 (2013).

⁹J. J. Brey, M. I. García de Soria, P. Maynar, and V. Buzón, "Homogeneous steady state of a confined granular gas," *Phys. Rev. E* **88**, 062205 (2013).

¹⁰J. J. Brey, P. Maynar, M. I. García de Soria, and V. Buzón, "Homogeneous hydrodynamics of a collisional model of confined granular gases," *Phys. Rev. E* **89**, 052209 (2014).

¹¹J. J. Brey, V. Buzón, P. Maynar, and M. García de Soria, "Hydrodynamics for a model of a confined quasi-two-dimensional granular gas," *Phys. Rev. E* **91**, 052201 (2015).

¹²J. J. Brey, V. Buzón, M. I. García de Soria, and P. Maynar, "Stability analysis of the homogeneous hydrodynamics of a model for a confined granular gas," *Phys. Rev. E* **93**, 062907 (2016).

¹³R. Soto, D. Risso, and R. Brito, "Shear viscosity of a model for confined granular media," *Phys. Rev. E* **90**, 062204 (2014).

¹⁴V. Garzó, R. Brito, and R. Soto, "Enskog kinetic theory for a model of a confined quasi-two-dimensional granular fluid," *Phys. Rev. E* **98**, 052904 (2018).

¹⁵V. Garzó, R. Brito, and R. Soto, "Enskog kinetic theory for a model of a confined quasi-two-dimensional granular fluid," *Phys. Rev. E* **102** (Erratum), 059901 (2020).

¹⁶V. Garzó, R. Brito, and R. Soto, "Stability of the homogeneous steady state for a model of a confined quasi-two-dimensional granular fluid," *EPJ Web of Conferences* **249**, 04005 (2021).

¹⁷M. Joyce, J. Morand, and P. Viot, "Attractor nonequilibrium stationary states in perturbed long-range interacting systems," *Phys. Rev. E* **93**, 052129 (2016).

¹⁸R. Maire, A. Plati, M. Stockinger, E. Trizac, F. Smalenburg, and G. Foffi, "Interplay between an absorbing phase transition and synchronization in a driven granular system," *Phys. Rev. Lett.* **132**, 238202 (2024).

¹⁹A. Plati, R. Maire, E. Fayen, F. Boulogne, F. Restagno, F. Smalenburg, and G. Foffi, "Quasi-crystalline order in vibrating granular matter," *Nature Physics* **20**, 465–471 (2024).

²⁰R. Maire and A. Plati, "Enhancing (quasi)-long-range order in a two-dimensional driven crystal," *J. Chem. Phys.* **161**, 054902 (2024).

²¹V. Garzó, R. Brito, and R. Soto, "Navier–Stokes transport coefficients for a model of a confined quasi-two dimensional granular binary mixture," *Phys. Fluids* **33**, 023310 (2021).

²²V. Garzó, R. Brito, and R. Soto, "Applications of the kinetic theory for a model of a confined quasi-two dimensional granular binary mixture: Stability analysis and thermal diffusion segregation," *Phys. Fluids* **36**, 033326 (2024).

²³V. Garzó, R. Brito, and R. Soto, "Erratum: "Applications of the kinetic theory for a model of a confined quasi-two dimensional granular binary mixture: Stability analysis and thermal diffusion segregation" [Phys. Fluids **36**, 033326 (2024)]," *Phys. Fluids* **36**, 049901 (2024).

²⁴S. Chapman and T. G. Cowling, *The Mathematical Theory of Nonuniform Gases* (Cambridge University Press, Cambridge, 1970).

²⁵T. Pöschel and T. Schwager, *Computational Granular Dynamics: Models and Algorithms* (Springer, Berlin, 2005).

²⁶M. P. Allen and D. J. Tildesley, *Computer Simulation of Liquids* (Oxford University Press, Oxford, 2017).

²⁷D. Frenkel and S. Berend, *Understanding Molecular Simulation: From Algorithms to Applications* (Elsevier, London, 2023).

²⁸G. A. Bird, *Molecular Gas Dynamics and the Direct Simulation Monte Carlo of Gas Flows* (Clarendon, Oxford, 1994).

²⁹V. Garzó and J. M. Montanero, "Diffusion of impurities in a granular gas," *Phys. Rev. E* **69**, 021301 (2004).

³⁰V. Garzó and F. Vega Reyes, "Mass transport of impurities in a moderately dense granular gas," *Phys. Rev. E* **79**, 041303 (2009).

³¹V. Garzó, "Brazil-nut effect versus reverse Brazil-nut effect in a moderately granular dense gas," *Phys. Rev. E* **78**, 020301 (R) (2008).

³²J. F. Lutsko, "Kinetic theory and hydrodynamics of dense, reacting fluids far from equilibrium," *J. Chem. Phys.* **120**, 6325 (2004).

³³R. Brito, R. Soto, and V. Garzó, "Energy nonequipartition in a collisional model of a confined quasi-two-dimensional granular mixture," *Phys. Rev. E* **102**, 052904 (2020).

³⁴V. Garzó, *Granular Gaseous Flows* (Springer Nature, Cham, 2019).

³⁵V. Garzó and J. W. Dufty, "Hydrodynamics for a granular binary mixture at low density," *Phys. Fluids* **14**, 1476–1490 (2002).

³⁶V. Garzó, J. W. Dufty, and C. M. Hrenya, "Enskog theory for polydisperse granular mixtures. I. Navier–Stokes order transport," *Phys. Rev. E* **76**, 031303 (2007).

³⁷V. Garzó, C. M. Hrenya, and J. W. Dufty, "Enskog theory for polydisperse granular mixtures. II. Sonine polynomial approximation," *Phys. Rev. E* **76**, 031304 (2007).

³⁸The term $-(p/\rho)(1+T\partial_T \ln p^*)(\partial f^{(0)}/\partial \mathbf{V})$ was neglected in the expression (47) of the quantity $\mathbf{A}(\mathbf{V})$ derived in Ref. 14. This term could give rise to a nonzero contribution to the kinetic thermal conductivity κ_k of the granular gas. However, when one takes the Maxwellian approximation to the zeroth-order distribution $f^{(0)}$, this contribution to κ_k vanishes. Thus, within this approximation, the expressions of the Navier–Stokes transport coefficients obtained in Ref. 14 remain unaltered.

³⁹J. T. Jenkins and F. Mancini, "Balance laws and constitutive relations for plane flows of a dense, binary mixture of smooth, nearly elastic, circular disks," *J. Appl. Mech.* **54**, 27–34 (1987).

⁴⁰T. M. Reed and K. E. Gubbins, *Applied Statistical Mechanics* (MacGraw-Hill, New York, 1973).

⁴¹J. M. Kincaid, E. G. D. Cohen, and M. López de Haro, "The enskog theory for multicomponent mixtures. IV. Thermal diffusion," *J. Chem. Phys.* **86**, 963–975 (1987).

⁴²V. Garzó, J. M. Montanero, and J. W. Dufty, "Mass and heat fluxes for a binary granular mixture at low density," *Phys. Fluids* **18**, 083305 (2006).

⁴³J. T. Jenkins and D. K. Yoon, "Segregation in binary mixtures under gravity," *Phys. Rev. Lett.* **88**, 194301 (2002).

⁴⁴J. J. Brey, M. J. Ruiz-Montero, and F. Moreno, "Energy partition and segregation for an intruder in a vibrated granular system under gravity," *Phys. Rev. Lett.* **95**, 098001 (2005).

⁴⁵J. J. Brey, M. J. Ruiz-Montero, and F. Moreno, "Hydrodynamic profiles for an impurity in an open vibrated granular gas," *Phys. Rev. E* **73**, 031301 (2006).

⁴⁶D. Serero, I. Goldhirsch, S. H. Noskowicz, and M. L. Tan, "Hydrodynamics of granular gases and granular gas mixtures," *J. Fluid Mech.* **554**, 237–258 (2006).

⁴⁷V. Garzó, "Segregation in granular binary mixtures: Thermal diffusion," *Europhys. Lett.* **75**, 521–527 (2006).

⁴⁸R. Brito, H. Enríquez, S. Godoy, and R. Soto, "Segregation induced by inelasticity in a vibrofluidized granular mixture," *Phys. Rev. E* **77**, 061301 (2008).

⁴⁹V. Garzó, "Thermal diffusion segregation in granular binary mixtures described by the Enskog equation," *New J. Phys.* **13**,

055020 (2011).

⁵⁰R. Gómez González and V. Garzó, “Tracer diffusion coefficients in a moderately dense granular suspension: Stability analysis and thermal diffusion segregation,” *Phys. Fluids* **35**, 083318 (2023).

⁵¹J. M. Montanero and A. Santos, “Monte Carlo simulation method for the Enskog equation,” *Phys. Rev. E* **54**, 438–444 (1996).

⁵²J. M. Montanero and A. Santos, “Simulation of the Enskog equation à la Bird,” *Phys. Fluids* **9**, 2057–2060 (1997).

⁵³D. C. Hong, P. V. Quinn, and S. Luding, “Reverse Brazil nut problem: Competition between percolation and condensation,” *Phys. Rev. Lett.* **86**, 3423–3426 (2001).

⁵⁴R. D. Wildman, J. M. Huntley, and D. J. Parker, “Granular temperature profiles in three-dimensional vibrofluidized granular beds,” *Phys. Rev. E* **63**, 061311 (2001).

⁵⁵A. P. J. Breu, H. M. Ensner, C. A. Kruelle, and I. Rehberg, “Reversing the Brazil-nut effect: Competition between percolation and condensation,” *Phys. Rev. Lett.* **90**, 014302 (2003).

⁵⁶T. Schautz, R. Brito, C. A. Kruelle, and I. Rehberg, “A horizontal Brazil-nut effect and its reverse,” *Phys. Rev. Lett.* **95**, 028001 (2005).

⁵⁷V. Garzó and F. Vega Reyes, “Segregation of an intruder in a heated granular gas,” *Phys. Rev. E* **85**, 021308 (2012).

⁵⁸V. Garzó, J. A. Murray, and F. Vega Reyes, “Diffusion transport coefficients for granular binary mixtures at low density: Thermal diffusion segregation,” *Phys. Fluids* **25**, 043302 (2013).

⁵⁹J. Qiao, C. Duan, K. Dong, W. Wang, H. Jiang, H. Zhu, and Y. Zhao, “Dem study of segregation degree and velocity of binary granular mixtures subject to vibration,” *Powder Technol.* **382**, 107–117 (2021).

⁶⁰V. Garzó, “Segregation by thermal diffusion in moderately dense granular mixtures,” *Eur. Phys. J. E* **29**, 261–274 (2009).

⁶¹L. Trujillo, M. Alam, and H. J. Herrmann, “Segregation in a fluidized binary granular mixture: Competition between buoyancy and geometric forces,” *Europhys. Lett.* **64**, 190–196 (2003).

⁶²M. Alam, L. Trujillo, and H. J. Herrmann, “Hydrodynamic theory for reverse Brazil nut segregation and the non-monotonic ascension dynamics,” *J. Stat. Phys.* **124**, 587–623 (2006).

⁶³M. G. Chamorro, R. Gómez González, and V. Garzó, “Kinetic theory of polydisperse granular mixtures: Influence of the partial temperatures on transport properties. A review,” *Entropy* **24**, 826 (2022).

⁶⁴A. Rosato, K. J. Strandburg, F. Prinz, and R. H. Swendsen, “Why the Brazil nuts are on top: Size segregation of particulate matter by shaking,” *Phys. Rev. Lett.* **58**, 1038–1040 (1987).

⁶⁵J. Duran, J. Rajchenbach, and E. Clément, “Arching effect model for particle size segregation,” *Phys. Rev. Lett.* **70**, 2431–2434 (1993).